THE INTERACTIONS AND EXCHANGES OF METAL-BOUND SULFUR CONTAINING LIGANDS WITH VARIOUS TRANSITION METALS

A Thesis

by

WILLIAM SCOTT FOLEY

Submitted to the Office of Graduate Studies of
Texas A&M University
in partial fulfillment of the requirements for the degree of

MASTER OF SCIENCE

December 2009

Major Subject: Chemistry

THE INTERACTIONS AND EXCHANGES OF METAL-BOUND SULFUR CONTAINING LIGANDS WITH VARIOUS TRANSITION METALS

A Thesis

by

WILLIAM SCOTT FOLEY

Submitted to the Office of Graduate Studies of
Texas A&M University
in partial fulfillment of the requirements for the degree of

MASTER OF SCIENCE

Approved by:

Chair of Committee,	Marcetta Darensbourg
Committee Members,	Daniel Singleton
	François P. Gabbaï
	Mike Tice
Head of Department,	David Russell

December 2009

Major Subject: Chemistry

ABSTRACT

The Interactions and Exchanges of Metal-Bound Sulfur Containing Ligands with Various Transition Metals. (December 2009)

William Scott Foley, B.S., Texas A&M University

Chair of Advisory Committee: Dr. Marcetta Darensbourg

The treble clef binding motif of the zinc finger metalloprotein utilizes N_2S_2 binding sites. Whereas other N_2S_2 metalloproteins function in catalytic roles, zinc fingers serve mostly a structural element, although there has been some evidence that the zinc finger protein can interact with exogenous metal ions in aggregate formation or ion exchange. The work presented within has been aimed at precedents for both of the latter in Zn^{2+}.

The use of zinc and cadmium dithiolate complexes as mono- and bidentate S-donor ligands to tungsten carbonyl complexes was explored and the ability of zinc and cadmium complexes to stably bind to $W(CO)_x$ (x = 4 and 5) was established. The reactivity of thiolate sulfurs within the bimetallic complexes was examined, gaining an understanding of zinc and cadmium N_2S_2. The characteristics of these complexes were examined via IR, UV-vis, elemental analysis, and x-ray crystallography spectroscopy.

The ability of zinc to act as a scaffold for the synthesis of bisacetylbme-dach in the production and subsequent transfer of the same ligand to exogenous metal ion

sources was investigated. Cu^{2+} and Cd^{2+} analogs to the **Zn-1'-Ac$_2$** were synthesized and their properties investigated with IR, elemental analysis, and UV-vis spectroscopy.

ACKNOWLEDGEMENTS

I would like to thank my committee chair, Dr. Marcetta Darensbourg, and my committee members, Dr. Gabbaï, Dr. Singleton, and Dr. Tice, for their guidance and support throughout the course of this research.

Thanks also go to my friends and colleagues for providing support and encouragement. Without them, my time would not have meant as much to me. Specifically, I would like to thank Elky Almaraz who was a friend, mentor, and coworker who taught me much about both life and chemistry. Jason Denny also deserves my gratitude as he worked with me throughout most of my time and managed to stay a friend through it all. The whole of the MYD and DJD research groups were a constant source of information, levity, and inspiration; thank you.

Additionally, I would like to thank the department faculty and staff for all of their assistance in getting me through the many requirements along the way.

Small thanks go to Hironobu Sakaguchi, Tetsuya Takahashi, and Soraya Saga for their inspirational works that have played no small part in changing my life.

Fenrir and Carbuncle, I cannot express fully how much you two have affected my life.

Finally, thanks to my mother and father for their encouragement and to my siblings Dustin and Katie for their constant reminders to remain true to myself.

TABLE OF CONTENTS

LIST OF FIGURES

Page

LIST OF TABLES

1. INTRODUCTION

Zinc fingers, a protein family that is a part of the DNA transcription pathway amongst other functions, have recently become a focal point of various research topics.[1,2] The typical binding motifs for zinc fingers involve N-histidine and S-cysteine ligands arranged in a tetrahedral geometry about the zinc ion.[1] While there are motifs with N_1S_3 and S_4, the ZnN_2S_2 binding pattern is the most prevalent transcription factor found in nature.[1] The zinc ion does not directly interact with DNA during the transcription process, but instead serves as a structural scaffold that keeps the protein structure compact, engendering the proper fold for DNA binding.[3-7] Though the most commonly studied binding motif is the $ZnN_{His\ 2}\ S_{Cys\ 2}$, all N_2S_2 structures do not result in similar tertiary structures for proteins. In fact, there are eight different families of tertiary fold structures.[8] Although the first coordination sphere of the zinc(II) ion can be informative for structural analysis, the tertiary structure of the protein is responsible for the interactions of the protein with DNA and RNA.[9-11] As can be seen by Figure 1-1, the tertiary structure of one N_2S_2 Zinc finger protein wraps around the major groove of DNA with the major interactions comprised of H-bonding from Arginine and Histidine to guanine base pairs on DNA.[9-11] Thus, in order to best understand the function of zinc finger proteins, the first coordination sphere as well as the quaternary protein interactions must be investigated.

This thesis follows the style of *Inorganic Chemistry.*

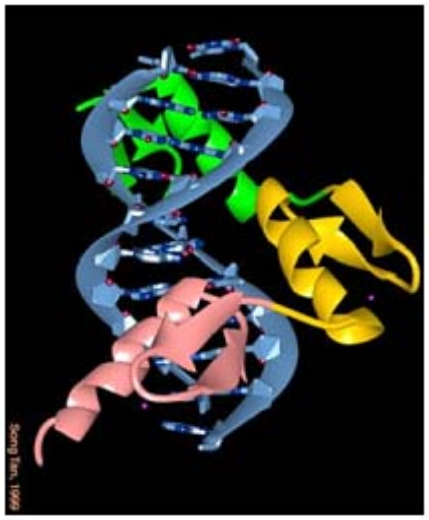

Figure 1-1. Zinc finger protein wrapping around the major groove of DNA. Modified from http://www.bmb.psu.edu/faculty/tan/lab/galler_protdna.html

The first coordination sphere of biological ligands is often approximated through the use of biomimetic small molecular synthetic equivalents, Figure 1-2. Such synthetic analogues as the dimeric bis(2-mercaptoethyl) -1,4-diazacycloheptane zinc(II) complex **[Zn-1']$_2$** have been shown to be useful in elucidating the relevance of thiol

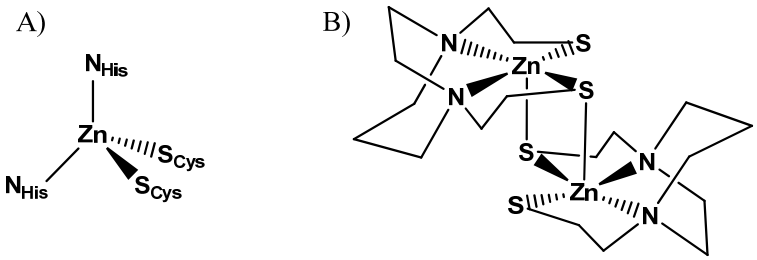

Figure 1-2. A structural comparison of (a) the treble clef zinc finger motif with a tetrahedral geometry as compared to the pseudo square planar (b) **[Zn-1']$_2$.**[1]

modification and the accessibility of varied oxidation states for other biological systems.[12-15] As these synthetic ligand sets only approximate naturally occurring donors from peptide sequences, developing new and assorted ligand sets is a constant goal in the process of understanding the natural systems.

The zinc(II) ion is found within the human body at the level of approximately 2-3 g and has been shown to play largely a structural function within proteins, although it is also responsible for several catalytic processes.[16, 17] Zinc finger proteins have commonly been observed with S_{cys}, N_{His}, and O donor atoms, displaying a versatility for both hard and soft ligands.[18, 19]

Although zinc is ubiquitous in natural systems, the development of synthetic analogues in new coordination spheres is challenging due to the lack of spectral signatures of zinc. That is, zinc(II) is a redox stable d^{10} metal ion and it is spectroscopically inactive to optical and EPR spectroscopy. While it is an option to utilize techniques such as ^{1}H-NMR, ^{13}C-NMR, and IR spectroscopies, these methods are limited by the ligand sets attached to the examined complex. The fluxional signals for the pendant arms and bridgeheads, such as those found in H_2bme-dach, make assigning individual peaks difficult.

Another way to examine zinc-containing proteins or mimetics is the attachment of a marker species that can be spectroscopically monitored so as to provide details about the desired analyte. Biomarker ligand complexes, such as metal carbonyls for example, might use characteristic IR stretching bands for the CO moieties that provide insight into the electronic properties of the biomimetic complexes.[16,17] Additionally, the

extended structure of biomarkers can also provide information about distant coordination spheres.[20] In our labs, nickel derivatives of the N_2S_2 ligand sets such as H_2bme-dach have been shown to readily attach metal carbonyl species forming adducts that have been characterized by infrared spectroscopy as well as x-ray diffraction studies or crystal structures.[20, 21]

Although zinc has been hypothesized to be purely a structural component of zinc fingers, there has been some evidence of metal ion exchange of the Zn^{2+} ion with Pt^{2+} as well as adduct formation to form bimetallic species. This has been observed in the presence of chemotherapeutic drugs such as Cisplatin.[20, 22] Additionally, zinc has also been proposed as a template for ligand formation for systems due to its thermodynamic and kinetic lability.[23] The examination of zinc ion exchanges with various other transition metal complexes proves enlightening for the further understanding of the function and properties of zinc in the proteins.

My research encompasses the synthesis of biomimetic complexes of the zinc containing units in zinc finger proteins as well as the examination of the interaction of these species with exogenous metal ions and metal-containing molecules. The zinc-containing biomimetic complexes will be utilized to study the reactivity of zinc-bound sulfur sites with exogenous metals. By using small molecular compounds that are structurally equivalent to metal-containing protein sites, the properties and chemical susceptibility towards metal exchange and the binding of metal-containing biomarkers is explored.

2. EXPERIMENTAL SECTION FOR SECTIONS

Abbreviations

H_2bme-dach : bis(2- mercaptoethyl) -1,4-diazacycloheptane

MeI : Methyl iodide

NaIAc : Iodoacetic acid sodium salt

Ni-1' : *N*,*N*′-Bis(2-mercaptoethyl)-1,4-diazacycloheptanenickel (II)

$[Zn\text{-}1']_2$: *N*,*N*′-Bis(2-mercaptoethyl)-1,4-diazacycloheptanezinc (II) Dimer

Zn-1'-Ac : [N-(3-Thiabutyl)-N'-(3-thiapentanoate)-1,4-diazacycloheptane]zinc(II)

Zn-1'-Ac_2 : 1,4-diazacycloheptane-1,4-diylbis(3-thiapentanoato) zinc(II),

Ni-1'-Ac : [N-(3-Thiabutyl)-N'-(3-thiapentanoate)-1,4-diazacycloheptane]nickel`(II)

Ni-1'-Ac_2 : 1,4-diazacycloheptane-1,4-diylbis(3-thiapentanoato) nickel(II)

$Pip_2W(CO)_4$: *cis*-dipiperidine tungstentetracarbonyl

Fc : ferrocene,biscyclopenyadienyl iron(II)

Fc* : bis-pentamethylcyclopentadienyl iron(II)

General Procedures and Physical Methods

Air sensitive reagents and complexes were handled under an inert atmosphere utilizing standard Schlenk techniques or in a glove box containing an Argon atmosphere. Solvents were purified according to standard procedures and were freshly distilled under N_2 prior to use or purified and degassed via a Bruker solvent system.[24] Reagents were purchased from commercial sources and used as received unless otherwise stated.

Solution based infrared spectroscopy spectra were recorded on a Bruker Tensor 27 FTIR using 0.1 mm CaF_2 sealed cells. The Pike MIRacle^{TM} attachment from Pike Technologies was used to obtain spectra via Attenuated Total Reflectance for solid samples.

UV-VIS spectra were collected with a Shimadzu UV-2450 spectrophotometer with 1 cm path length quartz cells to hold samples.

Cyclic Voltammograms were obtained under positive argon pressure at 22°C using a BAS100W potentiostat equipped with a 3.0 mm glassy carbon electrode, a platinum wire auxillary electrode, and a silver/silver nitrate reference electrode. Measurements were performed in a CH_2Cl_2 solution with .1 M solution of $[Bu_4N][BF_4]$ as the supporting electrolyte. Bis(pentamethylcyclopentadienyl)iron, Fc*, was used as an internal standard (-0.31 V) and values reported are relative to NHE.

^{1}H-NMR spectra were collected on a Mercury 300 system.

Elemental analyses were performed by Atlantic Microlab, Inc., Norcross, GA, USA. Electrospray ionization mass spectra (ESI-MS) were obtained from the Laboratory for Biological Mass Spectrometry at Texas A&M University.

Experimental Details for Section 3

Materials. *N*,*N*′-Bis(2-mercaptoethyl)-1,4-diazacycloheptanezinc (II) Dimer ([Zn-1']$_2$),[22] *cis*-(piperidine)$_2$W(CO)$_4$,[25] and bis(2-mercaptoethyl)-1,4-diazacycloheptane (H_2bme-dach)[12] were synthesized according to published procedures.

Synthesis of [tetraethylammonium]N,N'-Bis(2-mercaptoethyl)-1,4-diazacycloheptanezinc(II)-chloro, Tungsten Tetracarbonyl Complex, [Et_4N][(Zn-1'-Cl)W(CO)$_4$]. To a 100 mL Schlenk flask, a sample of **[Zn-1']$_2$** (0.154 g, 0.27 mmol) was degassed prior to the addition of 25 mL of dry CH_2Cl_2. To the cloudy white suspension was added Et_4NCl (0.101 g, 0.61 mmol) in 25 mL of dry CH_2Cl_2. After 10 minutes, a solution of *cis*-(pip)$_2$W(CO)$_4$ (0.265 g, 0.570 mmol) in 35 mL of CH_2Cl_2 was slowly cannulated into the stirring [Zn-1']$_2$ solution. After 3 h, the yellow solution was anaerobially filtered and the volume reduced in vacuo slightly before hexanes were added to precipitate a bright yellow powder. The yellow powder was isolated by anaerobic filtration, washed twice with benzene, and dried under a N_2 flow to yield 0.30 g (0.40 mmol, 74%), The yellow powder was dissolved in minimal CH_2Cl_2 and then layered with hexanes to yield X-ray quality crystals over the course of 2 to 3 days. IR (DMF, cm-1): ν(CO), 1988 (w), 1861 (s), 1836 (m), 1801 (m). IR (CH_2Cl_2, cm^{-1}): ν(CO), 1990 (w), 1863 (s), 1845 (m), 1800 (m). Elem. anal. Calcd (found) for $C_{21}H_{38}N_3S_2O_4C_{l1}W_1Zn_1$ (MW = 745.4 g/mol): C, 33.84 (33.04); H, 5.14 (5.38); N, 5.64 (5.44). Mp: 70-115 °C (dec) color change to brown; °C (dec) color change to black.

Synthesis of [tetraethylammonium]N,N'-Bis(2-mercaptoethyl)-1,4-diazacycloheptanezinc(II)-chloro, Tungsten Pentacarbonyl Adduct, $[Et_4N][(Zn\text{-}1'\text{-}Cl)W(CO)_5]$. A 100 mL Schlenk flask was charged with 0.165 g (0.22 mmol) of **$[Et_4N][(Zn\text{-}1'\text{-}Cl)W(CO)_4]$** and then degassed before 25 mL of dry CH_2Cl_2 was added. A light partial pressure of CO was applied to the headspace and the solution was allowed to stir for 24 h, after which the solution turned a slight orange color with a cloudy precipitate. The solution was filtered anaerobically but further isolation was not possible as the precipitate quickly turned brown and oily. IR (DMF , cm^{-1}): ν(CO), 2063 (w), 1920 (s), 1869 (m).

Synthesis of N,N'-Bis(2-mercaptoethyl)-1,4-diazacycloheptanecadmium(II), $[Cd\text{-}1']_x$. Under N_2, **H_2bme-dach** (0.708 g, 3.21 mmol) was dissolved in 20 mL MeOH, and sodium methoxide (0.372 g, 6.89 mmol) in 15 mL MeOH was slowly added. The solution was vigorously stirred for 2.5 h at 22°C. Under N_2, $CdCl_2$ (0.589 g, 3.21 mmol) dissolved in a mixture of 15 mL MeOH/5 mL deionized H_2O was rapidly added to the stirring solution. A white precipitate immediately formed. After stirring under an N_2 blanket overnight, the white solid was isolated by filtration in air, and washed two times with MeOH to yield, after drying *in vacuo*, 0.656 g (1.99 mmol, based on monomeric unit) of **Cd-1'** product (62.0 % yield). The product was dissolved in pyridine and layered with diethyl ether to yield colorless x-ray quality crystals. ESI-MS: $[M + Cl^-]^-$ *m/z* 696. Solid State ^{113}Cd NMR: 556 ppm. Elem.Anal.: C: 32.68 (32.83), H: 5.48 (5.51), N: 8.47 (8.42). decomposition range: 205 – 220 °C change from white to brown in color; 300 °C color change to black.

Synthesis of N,N'-Bis(2-mercaptoethyl)-1,4-diazacycloheptanecadmium(II), Tungsten Pentacarbonyl Complex, [(Cd-1')W(CO)$_5$]$_2$ Dimer. The *in situ* preparation of the (THF)W(CO)$_5$ was executed utilizing W(CO)$_6$ (0.320 g, 0.909 mmol) in 300 mL THF. The solution was photolyzed for 2 h under Ar to yield a clear golden solution. In a 500 mL Schlenk flask, the **Cd-1'** (0.296 g, 0.895 mmol) and Et$_4$NCl (0.151 g, 0.909 mmol) were degassed prior to addition of 125 mL of dry THF. A solution of (THF)W(CO)$_5$ in 300 mL THF was slowly cannulated into the stirring **Cd-1'** suspension. After approximately 8 h of stirring, complete conversion to product was indicated by IR spectroscopy. The clear, bright yellow solution was filtered anaerobically and hexanes were added to the filtrate to precipitate a yellow powder. The flask was placed at 7 °C to aid in further precipitation of product. The yellow solid was isolated via anaerobic filtration, washed twice with hexane, and dried under an Ar flow to yield 0.444 g (0.542 mmol, 60.5 %). ESI-mass spectrum: [M + Cl$^-$]$^-$ *m/z* = 691. IR (in THF, cm^{-1}): 2061 (vw), 1917 (s), 1869 (w). (in DMF, cm^{-1}): 2061 (vw), 1919 (s), 1864(w). decomposition range: 115 °C color change to brown; 150 °C dark brown; 240°C black solid.

X-ray Diffraction Analysis. The X-ray data for the three structures were obtained in the X-ray Diffraction Laboratory at Texas A&M University. Low-temperature (110 K) X-ray diffraction data were collected on a Bruker AXS APEX-II CCD-based diffractometer (Mo Kα radiation, λ =.71073 Å) for **[Et$_4$N][(Zn-1'-Cl)W(CO)$_4$]**. The [**Cd-1'**]$_x$ and **[(Cd-1')W(CO)$_5$]$_2$** structures were obtained on a Bruker D8 GADDS/MWPC three-circle X-ray diffractometer (Cu Kα radiation, λ =

1.541 84 A °), also operating at 110 K. The structures were solved by direct methods. H atoms were added at idealized positions and refined with fixed isotropic displacement parameters equal to 1.2 times the isotropic displacement parameters of the atoms to which they were attached. Anisotropic displacement parameters were determined for all non-H atoms. The programs utilized were as follows: data collection and cell refinement for, *SHELXTL*;[26] data reduction, *SAINT*;[27] absorption correction, *SADABS*;[28] structure solution and structure refinement for all structures, *SHELXS-97* and *SHELXL-97*;[26] molecular graphics and preparation of material for publication, *SHELXTL-PLUS*, version 6.14.[26] The final data presentation and structure plots were performed using *X-Seed*.[29] The $[\mathbf{Cd\text{-}1'}]_x$ structure was solved by Dr. Reibenspies and $\mathbf{[(Cd\text{-}1')W(CO)_5]_2}$ by Dr. Bhuvanesh.

Experimental Details for Section 4

Materials. *N*,*N*′-Bis(2-mercaptoethyl)-1,4-diazacycloheptanezinc (II) Dimer ([Zn-1']$_2$),[22] *N*,*N*′-Bis(2-mercaptoethyl)-1,4-diazacycloheptanenickel (II) (Ni-1'),[12] 1,4-diazacycloheptane-1,4-diylbis(3-thiapentanoato) zinc(II), (Zn-1'-Ac$_2$),[30] 1,4-diazacycloheptane-1,4-diylbis(3-thiapentanoato) nickel(II), (Ni-1'-Ac$_2$),[30] [N-(3-Thiabutyl)-N'-(3-thiapentanoate)-1,4-diazacycloheptane]zinc(II), (Zn-1'-Ac),[20] and bis(2-mercaptoethyl) -1,4-diazacycloheptane (H_2bme-dach)[12] were synthesized as reported in the literature.

Reaction of [Zn-1']$_2$ with Nickel(II) tetrafluoroborate. Ni(BF_4)$_2$ was dried in vacuo before using. A sample of **[Zn-1']$_2$** (.088 g, 0.16 mmol) was added to a 100 mL Schlenk flask which was then degassed before 10 mL of dry MeOH was added. Ni(BF_4)$_2$ (.096 g, 0.41 mmol) in 10 mL dry MeOH was added via cannula to the white suspension. As various precipitation methods failed to yield solid product, the oily orange residue obtained upon reduction of solvent was used in subsequent analyses.

Attempted reaction of Ni-1' with Zn-1'-Ac$_x$ (x = 1 or 2). A sample of **Ni-1'** (.450 g, 1.63 mmol) was added to a 100 mL Schlenk flask which was then degassed before 20 mL of dry MeOH was added. One equivalent of Zn-1'-Ac$_x$ (x = 1 or 2) in 25 mL dry MeOH was added via cannula to the brown slurry. No reaction was observed at 22°C or at 65°C after 48 h.

Synthesis of 1-mercaptoethyl, 4-methyl-ethylmercaptoether, 1, 4-diazacycloheptanenickel (II) iodide, ([MeNi-1'][I]). A sample of **Ni-1'** (0.01 g, 0.036 mmol) was added to a 100 mL Schlenk flask which was then degassed before 30 mL of

dry MeOH and a 0.1 mL aliquot of 0.72 M MeI (0.072 mmol) in MeOH was added. The solution developed a light yellow color and ESI-M/S indicated the solution contained **[MeNi-1'][I].** ESI-MS: $[M]^+$ *m/z* 291.

Reaction of [MeNi-1'][I] with Zn-1'-Ac$_x$ (x = 1 or 2). The solution of **([MeNi-1'][I]** was used *in situ* as prepared previously. To the solution of **([MeNi-1'][I]** was added 1 equivalent of Zn-1'-Ac$_x$ (x= 1 or 2) in 15 mL dry MeOH via cannula. The resulting solution turns a rich green color over 8 h. The solution was filtered anaerobically and solvent was partially removed before addition of dry diethyl ether precipitated a green powder. The powder was washed three times with ether and then dried under N_2. ESI-MS: $[M]^+$ *m/z* 349.

Screenings of M^{n+} (n = 1, 2, 3)[M^{1+} = Ag^{1+}, Cu^{1+};M^{2+}= Cd, Co, Cu, Fe, Ga, Gd, Hg, Mn, Mg, Pb; M^{3+} = Fe^{3+}] reactivities with Zn-1'-Ac$_x$ (x = 1 or 2). These screenings were treated as air stable reactions. $AgNO_3$, Cu(acetate), $CdCl_2$, $CoSO_4$, $CuSO_4$, Fe(II)SO_4, Ga$(NO_3)_2$, Gd$(NO_3)_2$, HgI_2, Mn$(NO_3)_2$, $MgSO_4$, Pb(acetate)$_2$, and Fe(III)Cl_3 salts were used as received commercially. Sample of the metal salts (ca. 10 mg) were added to test tubes and dissolved in minimal amounts of MeOH. Initial colors, RF values in 1:1 MeOH:CH_3CN, and UV-vis spectra were acquired before 1 equivalent of **Zn-1'-Ac$_1$** was added from a stock solution of .25 M Zn source and all characterizations were repeated. This entire procedure was repeated with **Zn-1'-Ac$_2$**. A complete list of all the reagents used is found in Table 4-1.

Synthesis of 1,4-diazacycloheptane-1,4-diylbis(3-thiopentanoto)disodium, (Na$_2$1'-Ac$_2$), bisacetylbme-dach sodium salt, ligand directly. H_2bme-dach (0.44 g,

2.0 mmol) was placed in a 250 mL Schlenk flask in an Ar atmosphere and then 40 mL of dry MeOH was added. To this flask, sodium iodoacetate (NaIAc) (1.04 g, 5.0 mmol) in 40 mL dry MeOH was added. The very pale yellow solution was magnetically stirred for 18 h before it was used *in situ*. ESI-MS: $[M - Na]^-$ *m/z* 357.

Synthesis of 1,4-diazacycloheptane-1,4-diylbis(3-thiopentanoto) copper(II), (Cu-1'-Ac$_2$). The sodium salt of **(1'-Ac$_2$)$^{2-}$** was prepared as above. To the stirring ligand solution was added Cu(II)SO_4 (.318 g, 2.0 mmol) as a white slurry in 30 mL of dry MeOH. The solution remained as a white slurry until 10 mL deionized H_2O was added dropwise. The solution adopted a strong blue color over 20 h. The solution was filtered anaerobically and the filtrate was reduced under vacuo partially before ether was added to precipitate a blue powder. The blue powder was isolated anaerobically and washed twice more with small amounts of ether. The product was partially soluble in ether and some material was lost. The powder was redissolved in MeOH and chromatographed through a silica column with MeOH as the eluent. The blue fractions were collected and the solvent was removed to yield 0.158 g (0.40 mmol, 20 %). ESI-MS: $[M+H^+]^+$ *m/z* 398. IR (CH_2Cl_2, cm-1): ν(CO), 1631 (s), 1348 (w), 1327 (w). UV-Vis: (CH_3OH): $\lambda_{max.}$ nm, (ε, M^{-1} cm^{-1}) = 607(202), 348(2660), 287(1560). Evans Method: 1.46 B.M. Elem. anal. Calcd (found) for $C_{13}H_{22}N_2S_2O_4Cu_1H_2O$ (MW = 415.0 g/mol): C: 37.53 (37.04); H; 5.33 (5.76); N; 6.73 (6.64). Mp: 120 °C (dec) color change to green-brown; 200°C (dec) color change to black.

Synthesis of 1,4-diazacycloheptane-1,4-diylbis(3-thiopentanoto) cadmium(II), (Cd-1'-Ac$_2$). **Na$_2$1'-Ac$_2$** was prepared as above. To the stirring ligand

solution was added $Cd(NO_3)_2$ (0.474 g, 2.0 mmol) as a clear solution in 30 mL of dry MeOH. The solution became a white slurry. The solution was filtered anaerobically and the filtrate was partially reduced in vacuo before ether was added to precipitate a white powder. The powder was isolated anaerobically and washed twice more with small amounts of ether. The product is partially soluble in ether and some material was lost during the washing. The powder was redissolved in MeOH and chromatographed through a silica column with MeOH as the eluent. The fractions containing product, as determined by TLC of the fractions (the product has an RF value of 0.25 in 1:1 MeOH: CH_3CN), were collected and the solvent was removed under vacuum to yield 0.215 g (0.48 mmol, 48 %). ESI-MS: $[M+H^+]^+$ *m/z* 449. IR (ATR, cm-1): ν(CO), 1710 (s), 1359 (m), 1221 (m). Mp: 90-100 $^{\circ}$C (dec) color change to yellow-brown; 225°C (dec) color change to black.

3. $M(CO)_X$ ADDUCTS OF ZINC (II) AND CADMIUM (II) BIOMIMETIC COMPLEXES*

Inorganic biomimetics have aided the identification of structure and mechanism of metal containing proteins such as nickel superoxide dismutase (SOD), acetyl co-A synthase, nickel iron hydrogenase ([NiFe]H_2ase), diiron hydrogenase ([FeFe]H_2ase), and numerous other species.[31-33]

Rudimentary zinc finger models using the ligand sets of *N*,*N*‘-Bis (2-mercaptoethyl)-1,4-diazacycloheptane (H_2bme-dach) and *N*,*N*‘-Bis(2-mercaptoethyl)-1,4-diazacyclooctane (H_2bme-daco) have been studied.[22, 34] Figure 3-1 displays some early zinc finger models synthesized by our group. Of note, these compounds are dimeric in nature with thiolate sulfurs bridging to neighboring zinc centers. Each zinc center is pentacoordinate and displays intermediate square pyramidal geometries/trigonal bipyramidal geometries with τ values of .47, where τ is a measure of relative square pyramidal (value of 0) or trigonal bipyramidal (value of 1).[35] These compounds have been examined for their interactions with platinum-DNA synthetic analogues.[22] The thiolates of the zinc complexes showed reactivity towards the Pt^{2+} ion for both Zn-S-Pt adduct formation and for Zn/Pt metal exchange.

---

*Reproduced in part with permission from Almaraz, E.; Foley, W.S.; Denny, J.; Reibenspies, J.; Golden, M.; Darensbourg, M.Y. Inorg. Chem., **2009**, *48*, 5288-95. Copyright 2009. American Chemical Society.

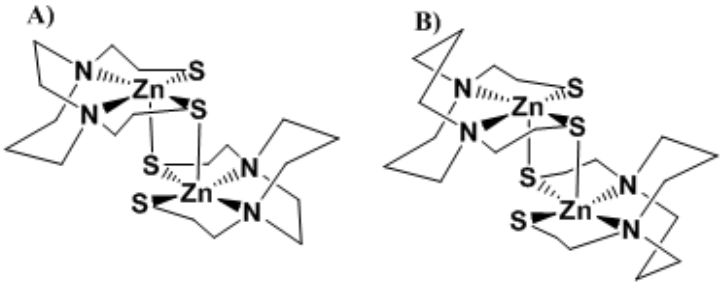

Figure 3-1. (a) *N*,*N*′-Bis(2-mercaptoethyl)-1,4-diazacycloheptanezinc (II) Dimer ($[Zn\text{-}1']_2$) and *N*,*N*′-Bis(2-mercaptoethyl)-1,4-diazacyclooctanezinc (II) Dimer ($[Zn\text{-}1]_2$).

Due to zinc being spectroscopically silent, biomarkers that bind through the reactive $S_{thiolate}$ donor atoms have been developed. Tungsten carbonyl complexes ensure that the interaction will be through bonding of a thiolate sulfur to the low-valent Tungsten and metal exchange would be avoided. Well-characterized Zn-$S_{thiolate}$ bound $W(CO)_x$ adduct species demonstrate that the CO band patterns and positions are suitable spectroscopic monitors.

Because of its NMR active nucleus, cadmium has been used to substitute for zinc, assuming similar or identical structures.[36] Thus, zinc can be exchanged for cadmium and some properties can be gleaned from the analog. Nevertheless, it has been cautioned by D.J. Darensbourg, *et al*. that cadmium can adopt geometries different from the zinc complexes it is intended to mirror.[37] Further research into the discrepancies between zinc-bound N_2S_2 complexes and analogous cadmium complexes can be informative regarding the toxic properties of cadmium when it substitutes for zinc in nature, and, by comparison of the differences, may further illuminate the role and reactivity of zinc fingers in biology.

The work presented herein was performed in collaboration with Elky Almaraz and Jason Denny and portions of it have been published already.[20]

Characterization of $[Et_4N][(Zn\text{-}1'\text{-}Cl)W(CO)_4]$. The **$[Zn\text{-}1']_2$** proved to have sufficiently strong Zn(II) – S intermolecular bonds that simple addition of $(Pip)_2W(CO)_4$ would not yield the μ-dithiolate bridging species of its own accord. The **$[Zn\text{-}1']_2$** dimer has limited solubility in MeOH; however, addition of tetraethylammonium chloride in a stoichiometric ratio to the white Zn solid solubilizes it, creating a clear colorless solution. This soluble intermediate was unisolable, yielding dimeric starting material in repeated attempts. The structure of the intermediate is hypothesized, Figure 3-2, from the final product obtained from the reaction of the intermediate with $(Pip)_2W(CO)_4$ to yield **$[Et_4N][(Zn\text{-}1'\text{-}Cl)W(CO)_4]$**, Figure 3-3**.** Crystals of **$[Et_4N][(Zn\text{-}1'\text{-}Cl)W(CO)_4]$** suitable for x-ray diffraction were obtained from layering hexanes onto a solution of **$[Et_4N][(Zn\text{-}1'\text{-}Cl)W(CO)_4]$** in CH_2Cl_2.

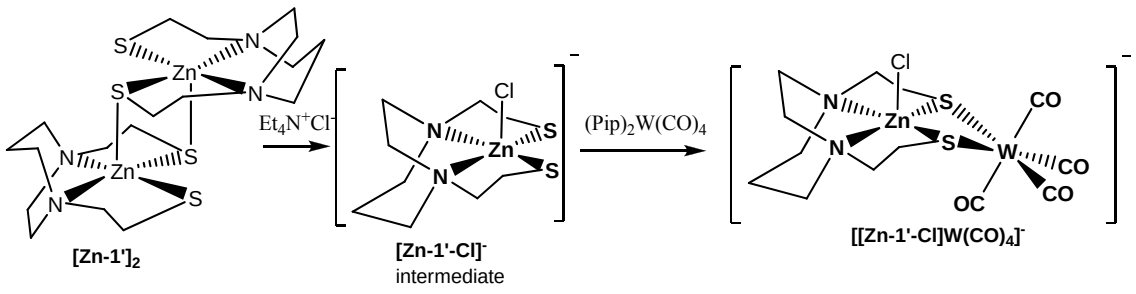

Figure 3-2. Reaction route to **$[Et_4N][(Zn\text{-}1'Cl)W(CO)_4]$**.

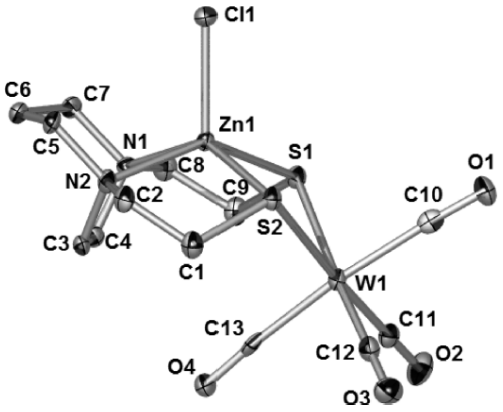

Figure 3-3. Molecular structure of **[Et_4N][(Zn-1'-Cl)$W(CO)_4$].** Selected bond distances (Å): Zn-N: 2.207(4); Zn-S_W: 2.39(1) ; W-S: 2.591(2) ; Zn-Cl: 2.290(1) ; W-CO (eq): 1.955(5) ; W-CO (ax): 2.025(3); Zn displacement from N_2S_2 plane: .744 ; Zn-W: 3.51. Selected bond angles (°): C^{10}-W-C^{13}: 173.5 ; S-Zn-S: 90.84 ; N-Zn-N: 73.21 ; hinge angle between best N_2S_2 plane and best WS(1)S(2)C(11)C(12) plane: 125°.

The molecular structure of the **[(Zn-1'-Cl)$W(CO)_4$]$^-$** anion is given in Figure 3-3. Selected metric parameters are reported in the caption of Figure 3-3 and at the end of this section. Notable features include the displacement of Zn^{2+} from the N_2S_2 plane by 0.744 Å with Zn-S distances of 2.457 Å. Both of these distances are shorter than literature values reported for a similar $[(Zn\text{-}1'\text{-}Cl)(Pt(dien))]^{+}$.[22] The hinge angle of 125° defined for the intersection of the N_2S_2 plane (without the zinc) with the equatorial plane of the tungsten complex, i.e. $W(S)_2C_2$, was larger than the Pt analog, 107.2°. Note the S-Zn-S bond angle of 90.84° and the N-Zn-N angle of 73.21°. The characterization by IR spectroscopy can be found below with tabulated values reported on page 24.

Characterization of [Et_4N][(Zn-1'-Cl)$W(CO)_5$]. The reaction solution of **[Et_4N][(Zn-1'-Cl)$W(CO)_4$]** in CH_2Cl_2 was found to develop new IR CO stretching bands when left to stir for longer than 24 h. In pattern and position, the new absorptions

were characteristic of M(μ-SR)W(CO)$_5$.[38] Allowing the reaction to continue for extended periods of time yielded a mixture of MCO products as identified by IR spectroscopy. In order to isolate the 5-coordinate zinc-tungsten adduct, **[Et$_4$N][(Zn-1'-Cl)W(CO)$_4$]** was synthesized *in situ* and CO was bubbled through the solution. The conversion was monitored via IR spectroscopy, Figure 3-4. While bands grew in for the W(CO)$_5$ complex, there was no evidence of the formation of other MWCO complexes. Additionally, the reaction did not proceed to completion, but instead displayed loss of CO after 72 hours. A monodentate Zn(μ-SR)W(CO)$_5$ was synthesized by others using the **[Zn-1']$_2$** as a starting material and then acetylating one of the thiolate sulfurs per zinc moiety, leaving only one sulfur available to bond to the W(CO)$_5$.[20]

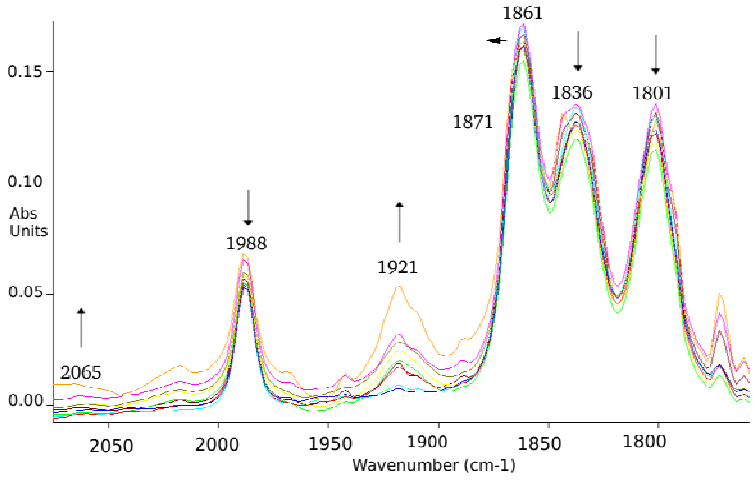

Figure 3-4. DMF solution IR spectra ν(CO) region of **[Et$_4$N][(Zn-1'-Cl)W(CO)$_4$]** during 1 atm CO gas addition over the course of 1 day at 22 ºC. Monitored conversion from [(Zn-1'-Cl)W(CO)$_4$]$^-$ (1988, 1861, 1836, 1801 cm^{-1}) to [(Zn-1'-Cl)W(CO)$_5$]$^-$ (2065, 1921, 1871 cm^{-1}).

Characterization of N,N'-Bis(2-mercaptoethyl)-1,4-diazacycloheptanecadmium(II), [Cd-1']$_x$. The preparation and isolation of the

cadmium analog to the previously described **[Zn-1']$_2$** species were identical in terms of experimental procedure. Analytically pure crystals were obtained from vapor diffusion of ether into methanol solution of **[Cd-1']$_x$** and were used for x-ray diffraction studies. The molecular structure of **[Cd-1']$_x$,** Figure 3-5 and crystal packing diagram, Figure 3-6**,** revealed a difference between the heavy metal analog and the zinc complex it was intended to mimic.

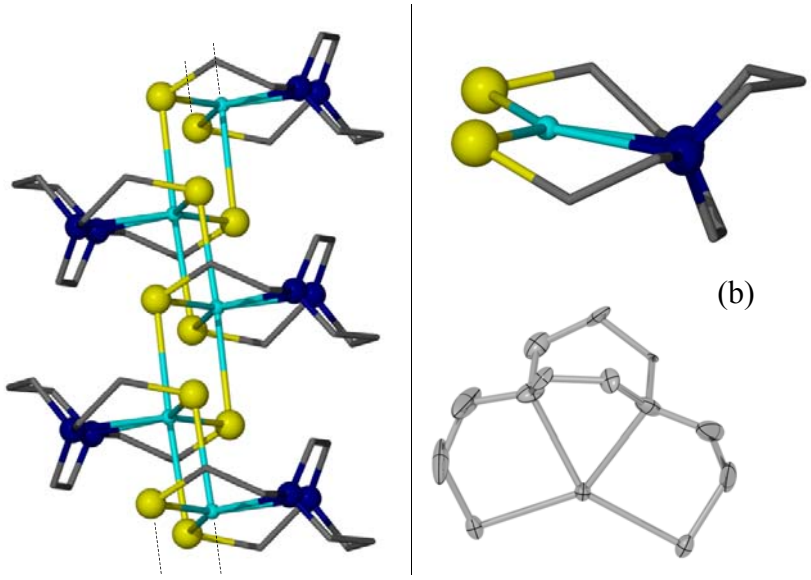

Figure 3-5. [Cd-1']$_x$ molecular structure. (a) Displays a five unit subchain of the extended chain polymeric complex. (b) A monomeric unit for closer inspection. (c) The thermal ellipsoid plot as seen from above the N_2S_2 plane. Disorder within the backbone carbons has been omitted and hydrogen atoms removed for clarity.

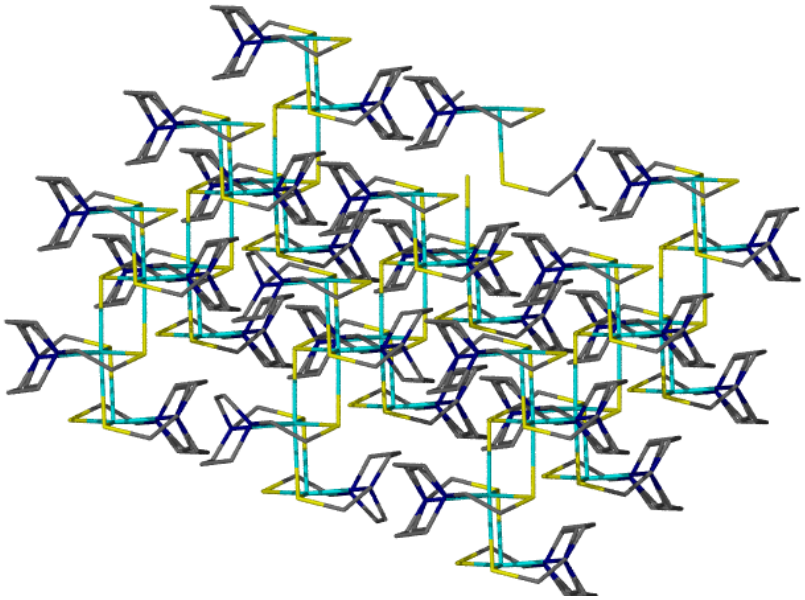

Figure 3-6. The crystal packing diagram for **[Cd-1']$_x$.** Disorder has been retained in the backbone.

i.e., the **Cd-1'** species is an extended chain polymer rather than a dimeric species like zinc. As to the strength of the Cd-S intermolecular bonds, tetraethylammonium chloride readily solubilized the white suspension when in MeOH, just as with the zinc analog. The **[Cd-1']$_x$** structure has some noteworthy features, as seen in the table on page 25. The S-Cd-S bond angle, at 132.5°, is larger by over 20° than any previously reported S-M-S angle with the **H_2bme-dach** ligand. The N-Cd-N angle is smaller than the zinc analog at 64.9° and 71.9°, respectively; this value is not substantially smaller than other reported N-M-N angles. The cadmium complex is able to facilitate the large change in the S-M-S bond with minimal change to N-M-N bond by twisting tetrahedrally by 20.24° (a tetrahedral twist is defined as the dihedral angle between the S-centroid of the N_2S_2 atom set-S plane and the N-centroid of the N_2S_2 atom set-N plane), disrupting the normally square planar geometry of the bme-dach ligand in the

N_2S_2 coordination sphere. The centroid of the N_2S_2 plane is utilized in favor of the Cd ion for calculating the planarity, or lack thereof, for the N_2S_2 donor set so that a uniform comparison can be made to later structures in which the Cd ion will be shown to be displaced from an otherwise idealized N_2S_2 plane. Also, it is clear from the structure presented that the Cd^{2+} is severely displaced from the centroid of the N_2S_2 binding site, making the use of the centroid more accurate in calculating the tetrahedral twist. The intermolecular Cd-S bonds are .28 Å longer than the intramolecular ones, which are 2.562 Å. The sulfur and nitrogen bonds are proportionally larger than their counterparts in the zinc dimer analog.

Characterization of $[(Cd\text{-}1')W(CO)_5]_2$. Attempts to prepare **$[Et_4N][(Cd\text{-}1'Cl)W(CO)_4]$** via the same procedure as for complex **$[Et_4N][(Zn\text{-}1'Cl)W(CO)_4]$** produced low yields (15%) of a $W(CO)_5$ adduct with the targeted $MW(CO)_4$ complex being a very minor product (5%). A direct synthesis of **$[(Cd\text{-}1')W(CO)_5]$** was developed based on $(THF)W(CO)_5$ as the tungsten carbonyl source, but yielded a dimeric **$[(Cd\text{-}1')W(CO)_5]_2$**, Figure 3-7**.**

The dimeric **$[(Cd\text{-}1')W(CO)_5]_2$** has some interesting features as detailed in Table 3-1 and seen in Figure 3-6. To begin, the tetrahedral twist seen in the **$[Cd\text{-}1']_x$** starting material is minimized yielding an almost perfect square plane (mean deviation .027 Å). The Cd ion was displaced above the N_2S_2 plane by .494 Å. Also, the intermolecular Cd-S distances are only .019 Å longer than their intramolecular equivalents (2.593 Å and 2.574 Å respectively). The S-Cd-S angle has decreased to

121° as well, though it is still over 10° larger than the largest S-M-S angle reported to have formed a bidentate ligand interaction to $W(CO)_4$.

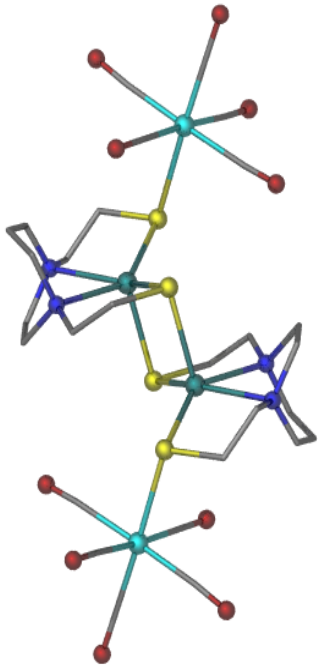

Figure 3-7. **$[(Cd\text{-}1')W(CO)_5]_2$** molecular structure. Select metric parameters provided below in Table 3-1.

Table 3-1. Selected bond lengths [Å] and angles [°] for **$[(Zn\text{-}1'\text{-}Cl)W(CO)_4]$**, **$[Cd\text{-}1']_x$** , **$[(Cd\text{-}1')W(CO)_5]_2$.**

	$[Zn\text{-}1']_2$	**$[(Zn\text{-}1'\text{-}Cl)W(CO)_4]^-$**	**$[Cd\text{-}1']_x$**	**$[(Cd\text{-}1')W(CO)_5]_2$**
M – N[a]	2.228(4)	2.207(4)	2.496(4)	2.40(2)
M(1) - $S_{M(1)}$[b]	2.308(2)		2.562(1)[a]	2.527(6)
M(1) – S_{Zn}[b]	2.496(2)			
M(1) – $S_{M(2)}$[c]	2.417(2)		2.842(1)[a]	2.593(6)
M(1) – S_W[b]		2.39 (1)[a]		2.574(6)
W-S		2.591(2)[a]		2.583(7)
∠S – M – S	108.28(6)	90.84(4)	132.50(5)	121.0(2)
∠N – M – N	71.9(2)	73.21(1)	64.9(2)	65.5(8)

M = Cd and Zn. [a] Average distance. [b] Intramolecular. [c] Intermolecular.

Conclusions for Section 3

The synthesis and characterization of these zinc- and cadmium-containing biomimetics offers insight into the geometric and electronic preferences of said metal ions and their affinities for sulfur in controlled, S-based aggregation. These are described below.

Interestingly, there is little difference in ν(CO) values between the anionic **[Zn-1'-Cl]**$^-$ as a monodentate donor to $W(CO)_5$ and the neutral **Zn-1'-Ac** -donor metalloligand previously synthesized.[20] We conclude that, in the latter, the modification of the thiolate to a thioether is compensated by the addition of the O donor to Zn, rendering the available thiolate S donor nearly as electron-rich as that in the anionic chlorozinc ligand.

The ν(CO) IR spectra of the tungsten carbonyl derivative, $M(\mu\text{-}SR)_2W(CO)_4$ and $M(\mu\text{-}SR)W(CO)_5$, display the requisite number of bands as predicted for idealized C_{2v} and C_{4v} symmetry, respectively.[38] Despite the severe asymmetry of the monodentate $[Zn\text{-}1'\text{-}Cl]^-$ ligand, the ν(CO) IR spectra are not distorted from that of a typical $LW(CO)_5$ in which L is a symmetrical ligand. This is not uncommon but, nevertheless, noteworthy.

A wide range of $Ni(N_2S_2)$ complexes have been well studied as metalloligands to tungsten carbonyl complexes and their ν(CO) frequencies were used to indicate their electron-donating abilities.[21, 39, 40] Data from these studies are included for comparison to the **[Zn-1'-Cl]**$^-$ Table 3-1. The four ν(CO) values for the anionic **[(Zn-1'-Cl)W(CO)$_4$]**$^-$ are positioned 8-16 cm^{-1} lower than those of the neutral $[(Ni\text{-}1')W(CO)_4]$ analog. This result is consistent with the overall charge on the heterobimetallic; notably, the dianionic

$[(Ni\text{-}ema)W(CO)_4]^{2-}$ [ema = N,N'-ethylenebis(2-mercaptoacetamide)] also has ν(CO) IR bands some 10 cm^{-1} lower.

Table 3-2. $LW(CO)_x$ IR CO stretches in DMF.

L-L W(CO)$_4$	**A_1^1**	**B_1**	**A_1^2**	**B_2**
[Zn-1'-Cl]$^-$	1988	1861	1836	1801
[Ni-1'][a]	1996	1873	1852	1817
[Ni-1*][b]	1996	1871	1857	1816
$[Ni\text{-}ema]^{2-}$ [c]	1986	1853	1837	1791
LW(CO)$_5$	**A_1^1**	**E**	**A_1^2**	
[Zn-1'-Cl]$^-$	2063	1920	1869	
[Cd-1']	2061	1919	1864	
[Ni-1']	2061	1920	1874	
[Zn-1'-Ac]	2059	1910	1867	

[a] [Ni-1'] = [N,N'-bis(2-mercaptoethyl)-N,N'-diazacycloheptane]nickel(II). [b] [Ni-1*] = [N,N'-bis(2-mercapto-2-methylpropane-N,N'-diazacyclooctane] nickel(II). [c] $[Ni\text{-}ema]^{2-}$ = [N,N'-ethylenebis(2-mercaptoacetamide)]nickel(II).[21, 39, 40]

Unlike any other unaltered MN_2S_2 thus far reported, the **$[Cd\text{-}1']_x$** complex forms a coordination polymer, **$[Cd\text{-}1']_x$**. Like many of the NiN_2S_2 complexes published[20,21], the **$[Cd\text{-}1']_x$** reacts with $W(CO)_x$ species yielding spectroscopic and structural features of significance to the M-thiolate aggregative ability.

The structures of **$[Cd\text{-}1']_x$** and **$[(Cd\text{-}1')W(CO)_5]_2$** as well as the previously synthesized **$[Zn\text{-}1']_2$** and **$[(Zn\text{-}1'\text{-}Ac)W(CO)_5]$**[20], illustrate an interesting difference between the cadmium and zinc structures. The goal of using cadmium (II) was the expectation that, as a Zn analog with an NMR active nucleus, it would display similar

geometric and electronic characteristics to those of zinc. Yet, the zinc N_2S_2 complex is a dimer that forms an unstable species when bound via monothiolate bridging to a tungsten carbonyl complex while cadmium is an extended chain coordination polymer in which cadmium is hexacoordinate, in an N_2S_4 coordination environment. This polymer breaks up in the presence of $W(CO)_5$ and forms a stable dimer in which the Cd is now pentacoordinate, maintaining 3 Cd-S bonds. The geometric differences are highlighted in Figure 3-8. As is easily seen by the overlay, there is little geometric similarity between the two complexes. The cadmium complex is nearly octahedral with only the slight twist in the MS_2N_2 equatorial plane while the zinc complex displays a hybrid geometry between trigonal bipyramidal and square pyramidal. As seen in part (b) of Figure 3-8, when viewed from above, there is a seemingly good semblance between the two cores with the zinc(II) being located closer to the centroid of the N_2S_2 plane, but with its axial sulfur bending far from the perfectly vertical sulfur on the cadmium complex.

(a) (b)

Figure 3-8. The **[Cd-1']$_x$** (silver) and **[Zn-1']$_2$** (blue) MN_2S_2 cores overlaid.

As for the electronic comparison of cadmium to zinc metallothiolates as ligands, there is very little difference in the IR spectra of the W(CO)x adducts, indicating similar donor abilities for the two. Additionally there are minimal differences between the Cd/Zn thiolates as ligand and the analogous nickel complexes shown in Table 3-2. One conclusion is that the $W(CO)_x$ reporter unit is insensitive to the neutral metallodithiolate ligands.

Through the analysis of the complexes synthesized herein, it can be seen that the zinc finger analogs can be attached to heavy metal biomarkers so as to monitor concentration of the zinc complex in solution. One problem that remains for the use of tungsten carbonyl complexes as biomarkers is the requirement for zinc to have only one available thiolate to bind to the tungsten carbonyl complex in order to achieve a stable bimetallic complex. As previous studies have shown, the thiolate sulfurs are primarily responsible for the zinc finger mimetic complexes' interactions with exogenous metals.[20,30]

The stable zinc/cadmium-tungsten carbonyl complexes have no remaining or available thiolate sulfurs. The **[(Zn-1'-Cl)W(CO)$_4$]** species is bound in a bidentate fashion via the sulfurs, leaving both thiolates tied up. Attempts to form the monodentate variant without first acetylating one of the thiolates into a thioester proved fruitless as the 'free' thiolate leaves the bimetallic complex too reactive. The presence of active thiolates that are free triggers CO loss and degredation.

[Cd-1']$_x$ is probably unable to form the bidentate adduct with W(CO)$_4$ due to the 133° S-Cd-S angle being too large. When **[(Cd-1')W(CO)$_5$]$_2$** was synthesized, the thiolate sulfur that is not engaged in bridging to the tungsten adduct retains an intermolecular bond with the Cd on an adjacent unit. Cadmium's ability to retain the thiolate bond from a neighboring unit where zinc cannot is due to the higher sulfophilicty of cadmium.

The increased reactivity of the zinc and cadmium complexes as compared to nickel analogs previously studied can be attributed to group 12 elements' tendency to leave the nucleophilicity of donor ligands intact. The thiolate sulfurs bound to group 12 metals remain as active as their free counterparts and this is reflected by the fact that all of the stable zinc and cadmium complexes with sulfur donor atoms have no free thiolate sulfurs.

4. ZINC ION EXCHANGE WITHIN $N_2S_2O_X$ (X = 1 OR 2) LIGAND SYSTEMS AND CHARACTERIZATION OF EXCHANGE COMPLEXES*

The zinc finger proteins have shown evidence for interaction with other metal ions, specifically platinum bound DNA equivalents.[41] Explorations into the nature of the zinc-platinum interaction have examined both S-bridged multimetallic adducts and metal exchange possibilities, shown in Figure 4-1.[22, 42] The ability of zinc to be displaced from a ligand set by another transition metal ion is of particular interest due to the presence of myriad transition metal ions within the human body. Iron is found at levels comparable to that of zinc while cobalt and copper are found in trace amounts, as much as three orders of magnitude less than zinc.[43]

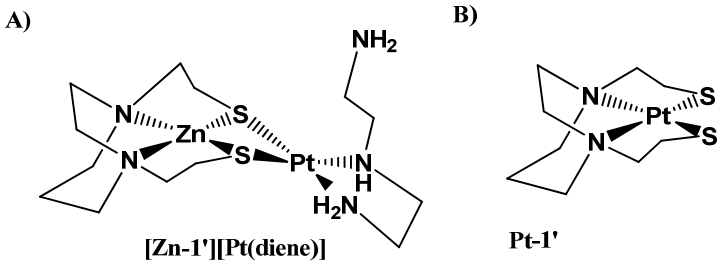

Figure 4-1. The zinc-platinum adduct (a) and the metal exchange product (b).

*Reproduced in part with permission from Almaraz, E.; Denny, J. A.; Foley, W.S.; Reibenspies, J. H.; Bhuvanesh, N.; Darensbourg, M. Y., Dalton Trans. In press. Copyright 2009. Royal Chemical Society.

Although the exchangeable ions are themselves ligated and not "free" or in a readily available form for metal exchange with zinc, the possibility of exchange remains, particularly under physiological stress or in the presence of excess mineral intake. Nature often displays similar ligand sets with different transition metals for various proteins and the change in the metal center alters the functionality of the protein.[33, 44-46] As Lindahl, *et al*, reported in their work, exchanging a nickel for a copper ion rendered the Acetyl coA Synthase enzyme inactive.[33]

As of now, zinc biomimetic complexes have been reacted with platinum and nickel complexes, Figure 4-2.[22] As the nickel part in Figure 4-2 indicates, the creation of the bisacetylbme-dach nickel, Ni-1'-Ac_2 has been performed from Ni-exchange into the Zn-scaffolded pre-formed ligand, (4) and (5), as well as by direct synthesis from Ni-1', (6). The two different pathways for the exchange differ in that pathway (5) forms the hexacoordinate ligand around the zinc and then exchanges it with the nickel. The other pathway, (4), forms a five coordinate complex around the zinc and, with addition of nickel at 0.5 equivalents, auto-cannibalizes one of the acetate arms from an ancillary complex to form the diacetate species along with reclamation of $[Zn\text{-}1']_2$. Due to the spectroscopic inactivity of zinc and its similar solubility properties to nickel when within the six coordinate ligand set, obtaining reliable yields and other analytical spectroscopic values has proven to be difficult from these pathways, thus necessitating pathway (6) for yield determination.

The lack of preference for specific coordination environments about the Zn^{2+} resulted in the facile formation of both the penta and hexacoordinate Zn^{2+} complexes. This finding led to the discovery of a novel feature of the penta-coordinate **Zn-1'-Ac**.

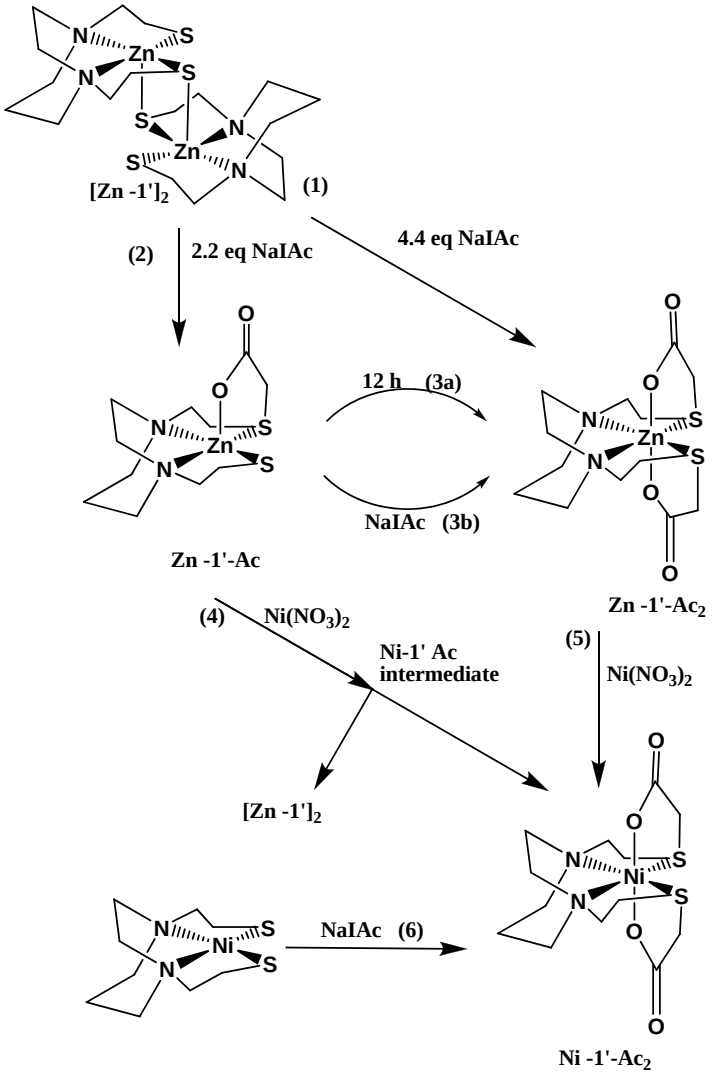

Figure 4-2. Previously studied reactions of zinc and nickel biomimetic pathways.[22]

When stirred in CH_3OH at 22°C over several hours, **Zn-1'-Ac** reformulates into the hexacoordinate **Zn-1'-Ac$_2$** and the dimeric **[Zn-1']$_2$** precursor from which it was originally synthesized (before alkylation by $Na^+[ICH_2CO_2]^-$), Figure 4-3. This self-reactivity or cannibalism was not explored in the well-studied Zn-1-Ac (the bme-daco) analog.[47] A related reaction is seen in the Zn/Ni transmetallation reactions shown in pathway (5) of Figure 4-2, which took place with rapid formation of the same **Ni-1'-Ac$_2$** product.

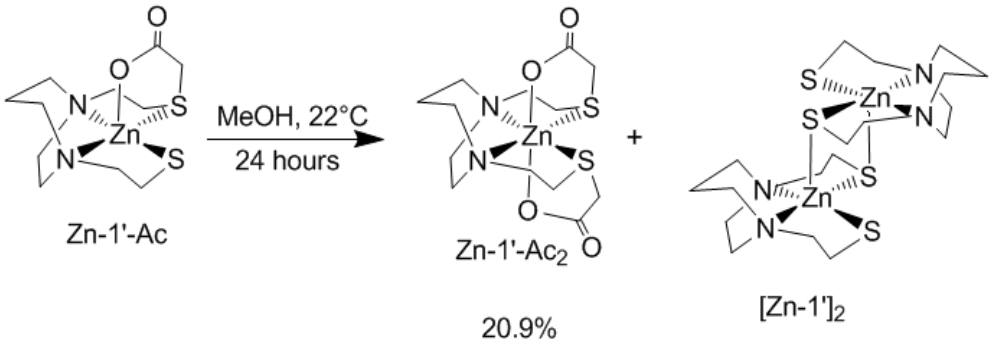

Figure 4-3. The ligand cannibalism of Zn-1'-Ac to form the diacetate species and the starting dimer.

Part of the work contained herein was completed in collaboration with Elky Almaraz and is published.[30]

Mechanistic insight for the ligand cannibalism to form M-1'-Ac$_2$. As Figure 4-2 illustrates, the **1'-Ac** ligand is capable of scavenging a second acetylate arm from other **Zn-1'Ac** complexes in order to form **M-1'-Ac$_2$**. Experiments that lead to mechanistic understanding of these exchange reactions are as follows: (1) as the BF_4^-

salt, Ni^{2+} does not exchange with Zn^{2+} in the **[Zn-1'$]_2$** dimer; rather, aggregates form that are presumably bridged by thiolate sulfurs; (2) if we hypothesize that the **Zn-1'-Ac** and **Zn-1'-Ac$_2$** serve as Ni–$S_{thiolate}$-alkylating agents, transferring the $^{+}CH_2CO_2^{-}$ units to available thiolates with the Zn-thiolate serving as a leaving group as does iodide in $ICH_2CO_2^{-}$, then the **Ni-1'**, should be an optimal receiver for $^{+}CH_2CO_2^{-}$ from the zinc carriers. As shown in the upper reaction attempted in Figure 4-4, this reaction failed. In contrast, the **[MeNi-1'][I]** complex shows reaction with **Zn-1'-Ac** yielding the blue-green mixed thioether compound. The implication of this lack of reactivity is discussed below. The product was characterized by ESI-mass spectrometry (a strong Ni-containing signal at *m*/*z*=349 corresponding to the methylated **Ni-1'-Ac** species was observed). The structure shown in Figure 4-3 is an analogue of the acetylated Ni(bme-daco)Me^{+} complex; however, the latter formed a blue coordination polymer whereas the **Ni-1'Ac Me^{+}** formed a green methanol solution.[47b]

Screens of M^{n+} (n = 1, 2, 3) [M^{1+} = Ag^{1+}, Cu^{1+}; M^{2+} = Cd, Co, Cu, Fe, Ga, Gd, Hg, Mn, Mg, Pb; M^{3+} = Fe^{3+}] reactivities with Zn-1'-Ac$_x$ (x = 1 or 2). The screening results according to products determined by ESI-MS and TLC can be seen in Table 4-1 and 4-2.

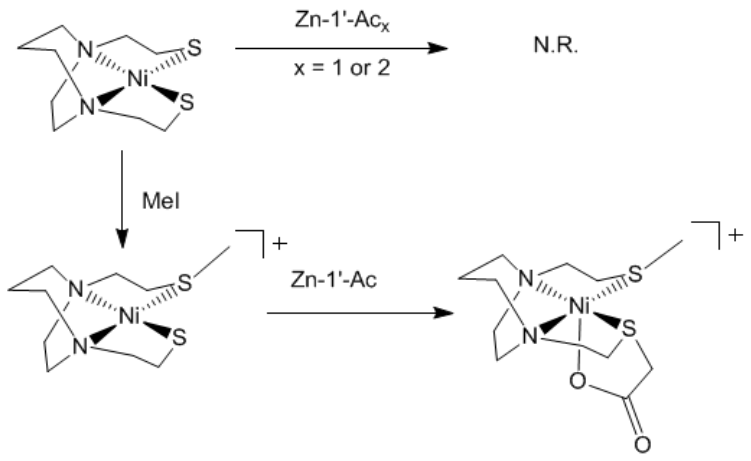

Figure 4-4. Reaction pathways to address the mechanism for ligand cannibalism and reformulation.

Table 4-1. Scope of Zn^{2+}/M^{n+} exchange reactions with Zn-1'-Ac_x (x = 1, 2)

Metal Source	x = 1	x = 2
$AgNO_3$	N.R.	N.R.
$CdCl_2$	N.R.	**Cd-1'-Ac_2**
$CoSO_4$	**Co-1'-Ac_2**	**Co-1'-Ac_2**
$CuSO_4$	**Cu-1'-Ac_2**	**Cu-1'-Ac_2**
Fe(II)SO_4	N.R.	Unknown
Fe(III)Cl_3	**Fe(II)-1'-Ac_2**	Unknown
$Ga(NO_3)_2$	N.R.	N.R.
$Gd(NO_3)_2$	N.R.	N.R.
HgI_2	Unknown	**Hg-1'-Ac_2**
$Mn(NO_3)_2$	N.R.	N.R.
$MgSO_4$	N.R.	N.R.
Pb(acetate)$_2$	N.R.	N.R.

Thus, the metals that directly exchanged were Cd^{2+}, Co^{2+}, Cu^{2+}, and Hg^{2+}, while Co^{2+}, Cu^{2+}, and Fe^{3+} evinced the aforementioned ligand cannibalism in order to yield the diacetylated species. Of particular interest is that not only did the Fe^{3+} reformulate the ligands, it also showed a change in the oxidation state of the ion. The Cu(I) reactions examined resulted in complicated oxidized product formation.

Table 4-2. Selected UV-vis results for metal exchanges.

Metal Source	Starting UV-vis signal (nm)	Reaction with Zn-1'-Ac	Reaction with Zn-1'-Ac_2
$AgNO_3$	---	---	280 (sh), 346 (sh)
$CdCl_2$	---	---	280, 315
$CoSO_4$	---	280, 458, 530, 570	280, 458, 530, 570
$CuSO_4$	248, 824	287, 348, 607	287, 348, 607
$Fe(II)SO_4$	297	---	---
$Fe(III)Cl_3$	231, 250, 302, 357	362	---
$Ga(NO_3)_2$	292	292	292
$Gd(NO_3)_2$	276	276	276
HgI_2	---	---	258, 298

Characterization of Cu-1'-Ac_2. The **Cu-1'Ac_2** complex was selected as the first goal for direct synthesis due to the clean ESI-MS spectrum from the Zn/Cu exchange approach. Synthesis of **Cu-1'** was not possible due to the formation of numerous side-products that were unseperable.[48] Due to this, the sodium salt of the **1'-Ac_2** ligand was synthesized directly. At first, NaOMe was used to deprotonate the thiols

of H_2bme-dach, but the base was found to degrade the ligand before it could be used. The addition of NaIAc to H_2bme-dach in MeOH produced the disodium salt of the ligand when reacted overnight. To make sure the free ligand was in fact the correct species, it was treated with $Ni(BF_4)_2$. This reaction yielded the **Ni-1'-Ac$_2$** complex, previously characterized.[30] A fresh sample of the free ligand was then treated with $CuSO_4$. The blue solution it yielded possessed identical spectroscopic properties to the **Cu-1'-Ac$_2$** produced from the metal exchange reactions.

The **Cu-1'-Ac$_2$** cyclic voltammograms, Figure 4-5 and 4-6, display the redox capabilities of the Cu^{2+} complex. The copper containing biomimetic displays a reversible redox couple centered at -671 mV representing a $Cu^{3+/2+}$ couple relative to the bis-pentamethylcyclopentadiene ferrocene couple at -310 mV. By comparison, it can be seen that the copper couple is a fully reversible reaction.

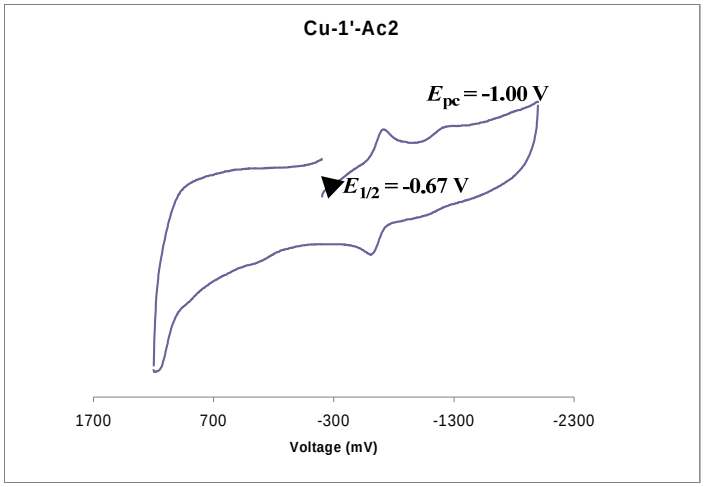

Figure 4-5. Cu-1'-Ac$_2$ cyclic voltammogram in CH_2Cl_2. Reversible $Cu^{2+/3+}$ at -.67 V and irreversible reduction at -1 V.

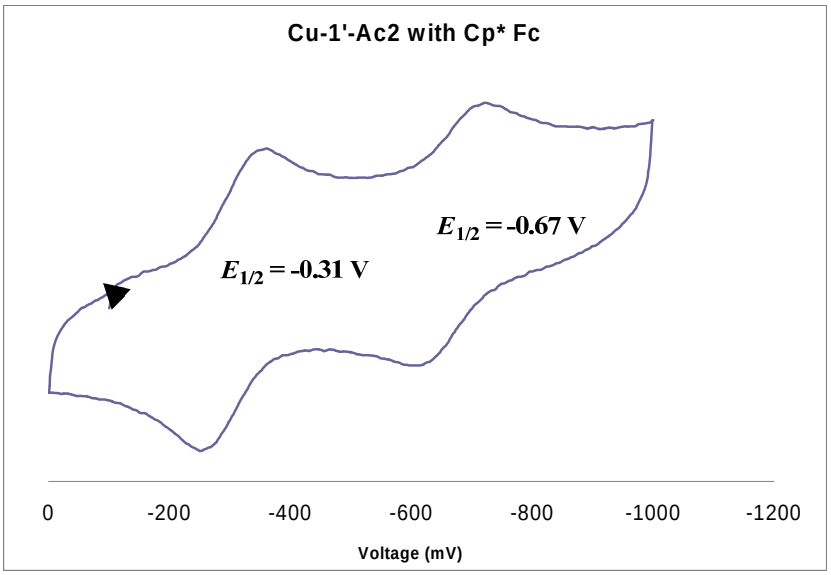

Figure 4-6. **Cu-1'-Ac_2** cyclic voltammogram in CH_2Cl_2 with Fc* added as a reference. The spectrum is zoomed in to highlight the $Cu^{2+/3+}$ couple and the Cp*Fc couple.

Characterization of Cd-1'-Ac_2. The cadmium species was chosen as a second choice for investigation because (1) it also appeared, via ESI-MS, to be a clean exchange and (2) it has biological relevance in comparison to the zinc complex. The direct full $N_2S_2O_2$ ligand synthesis approach, followed by metallation, as was done in the copper synthesis, proved to be the best route to Cadmium product. The product obtained possessed similar properties to the **Cd-1'-Ac_2** formed through Cd/Zn exchange.

Conclusions for section 4

The reactions described above lead us to conclude that the ligand exchange observed when Zn-1'-Ac_x (x = 1 or 2) is reacted with M^{2+} follows a path that uses the $O_{carboxylate}$ as an exogenous metal interaction site. The lack of reactivity of **[Zn-1']$_2$**

towards Ni^{2+} as compared to the rapid reaction of **Zn-1'Ac$_x$** (x = 1 or 2) is indicative of the need for a carboxylated "hook" in order to facilitate the unwrapping of the ligand.

Further, the results indicate that the acetylate arm cannibalism observed in the formation of M-1'-Ac_2 complexes is similarly facilitated by a M^{2+} - $O_{carboxylate}$ intermolecular interaction. Of significance to this conclusion is that the good nucleophile, NiN_2S_2 or **Ni-1'**, with cis-thiolates well known to be highly nucleophilic, does not rip out the $^{+}CH_2CO_2^{-}$ unit from Zn-1'-Ac_x. However, when the nickel is made more electrophilic as when one sulfur in **Ni-1'** is methylated, creating a positive charge on the nickel complex, cannibalization does occur. That is, although the single thiolate in **[MeNi-1'][I]** is deactivated, the positive charge on Ni^{2+} is more fully expressed, *i.e.* in the cationic complex, the thiolate is a poorer nucleophile but the nickel is a better electrophile.

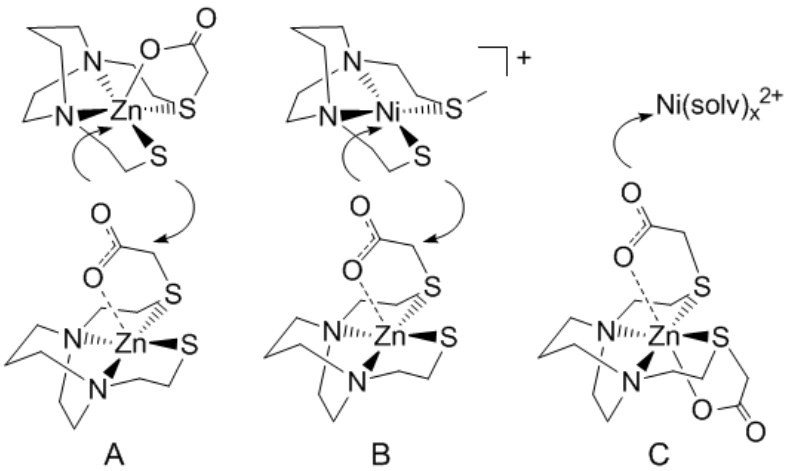

Figure 4-7. A and B: Proposed involvement of the carboxylate and thiolate in ligand cannibalism and acetate transfer. **C**: The nickel carboxylate interaction that begins unwrapping[dalt10–12] and ligand transfer from Zn^{2+} to Ni^{2+}.

For the reformulation of the **Zn-1**'**-Ac** complex, an adduct as shown in Figure 4-7, structure **A**, is suggested. Adduct **B**, is suggested for the positive result expressed in Figure 4-4. In addition, we suggest that the interaction of carboxylate oxygens of **Zn-1**'**-Ac$_2$** with nickel ions from the $Ni(BF_4)_2$ source, **C** of Figure 4-7, begins the unwrapping process that accounts for hexadentate $N_2S_2O_2$ ligand transfer from zinc to nickel in process (6) of Figure 4-2. While this unwrapping process undoubtedly involves multiple intermediates, none were spectroscopically observed.[49, 50]

The preliminary screenings of the interactions of Zn-1'-Ac_2 with exogenous metal ions revealed that simple salts of Cd^{2+}, Cu^{2+}, Co^{2+}, and Hg^{2+} undergo clean metal exchange to release zinc (II) from its hexacoordinate ligand set. Additionally, Cu^{2+} and Co^{2+} undergo a ligand cannibalism process when exchanged into a pentacoordinate ligand set in order to reformulate into a hexacoordinate metal complex. Finally, Cu^{1+} and Fe^{3+} displayed the aforementioned ligand scavenging as well as possible redox activity.

Table 4-3 illustrates the strong similarities in the acetate stretching region of the IR spectra for various M-1'-Ac_2 complexes. The copper and cadmium complexes fit in nicely with the other metal ion complexes, revealing a similar electronic effect on the acetate stretching region.

Table 4-3. M-1'-Ac_2 IR acetate stretching region, cm^{-1}, in CH_2Cl_2 except where noted.

M^{2+}	A	B	C
Zn^{2+}	1630	1350	1331
Ni^{2+}	1625	1348	1333
Cu^{2+}	1631	1348	1327
Co^{2+}	1626	1348	1329
Cd^{2+} [a]	1710	1359	1221

[a] spectrum recorded on solid sample by ATR-FTIR

The direct synthesis of **Cu-1'-Ac_2** and **Cd-1'-Ac_2** complexes revealed an interesting aspect of the 1'-Ac_2^{2-} ligand set. Copper (II) was unstable in the 4-coordinate N_2S_2 ligand set of bme-dach^{2-} and **Cu-1'-Ac_2** could not be synthesized by ligand-based acetylation as were zincc(II) and nickel(II). Indeed, the only way to maintain copper(II) stably within the ligand set was to either synthesize the ligand completely before adding the copper ion or to exchange the copper into the zinc-bound ligand set.

Through this research, we have come to an understanding of what ligand/metal properties must be present to achieve the metal ion exchange and the ligand cannibalization. The sulfur modification on a M-N_2S_2 by alkylation is necessary in order for the complex to scavenge an acetate arm off of a donor complex. Additionally, the carboxylate oxygens are responsible for the interaction with free metal ions in order to proceed with the ligand unwrapping and ion exchange process. This knowledge can help design future ligand sets as well as guide design of ion exchange processes with similar ligands.

5. CONCLUSIONS

The use of small molecular biomimetic complexes as structural and functional mimics for metalloproteins continues to grow as a field of study that aims to gain new understanding about the naturally occurring systems.[31,32] One downside to the use of synthetic analogs is that they have yet to display an ability to completely mimic the function that the metalloprotein carries out and have, as of so far, only displayed structural similarities and some electronic and spectroscopic semblances. Typically, the catalytic rates of biomimetics of enzyme active sites are orders of magnitude lower than naturally occurring enzymes.[51]

Metal containing proteins are often ligated by N, O, and S donors from amino acids, typically by the side chain residues. A common binding motif seen in various different protein systems is a MN_2S_2, appearing in complexes such as nickel superoxide dismutase, nitrile hydratase, acetyl coA synthase, and zinc fingers.[1,52-55] While maintaining these diverse donor atoms to metal ions, the metalloproteins are not only stable and soluble in aqueous solutions, but also capable of varied catalytic processes with rates that surpass industrial catalysis. Obviously, if this elegance of structure and function could be harnessed via easy to obtain synthetic analogs, it would offer great potential to numerous fields.

Zinc-containing proteins have displayed functional roles in biology for binding exogenous metal ions to form aggregate complexes, zinc-metal ion exchange, and even as a scaffold for the in vitro synthesis of ligands.[20, 22, 23] The diversity of roles that

zinc(II) can play in biological systems arises from its chemical inertness, being a d^{10} metal ion, and from the range of ligand donor atoms ligating it. Sulfur donor atoms often display reactivity towards aggregate formations, alkylation, and other electrophilic addition-type reactions. Additionally, zinc(II) is kinetically labile and also able to adopt a variety of geometries.

The synthesis and characterization of the zinc-tungsten bimetallic complex as well as the analogous studies of cadmium complexes has furthered the insight of zinc chemistry and the replacement of zinc with cadmium for spectroscopic techniques.

1) The ZnN_2S_2 and CdN_2S_2 metallothilate complexes as ligands are good electron donors, as established by ν(CO) spectroscopy.

2) Their ability to bind as mono- or bidentate is severely limited as compared to nickel containing analogs.

3) Using cadmium as an analog to zinc provided similar electronic data, but very different geometric data.

The ν(CO) reporter data found that the **[(Zn-1'-Cl)W(CO)$_4$]$^-$** complex ion displayed similar electronic properties to those revealed in studies of neutral NiN_2S_2 complexes bound via a bidentate fashion to tungsten carbonyl complexes. Unexpectedly, the presence of the negatively charged chloride as an apical donor ligand in **[(Zn-1'-Cl)W(CO)$_4$]$^-$** does not enhance the amount of negative charge donated to $W(CO)_4$. Similarly, the cadmium N_2S_2 analog complex as a monodentate donor ligand

to $W(CO)_5$ shows similar donor properties as to the NIN_2S_2 as a monodentate donor to $W(CO)_5$.[21]

This work provides new information for this field in terms of demonstrating the strong preference for zinc and cadmium N_2S_2 complexes not to have free thiolates. Whereas the nickel analogs synthesized previously were observed as both mono- and bidentate ligands to W(CO)x complexes, zinc(II) with two thiolate donors has, as of now, only been observed as a bidentate ligand to $W(CO)_4$ with any reasonable stability. The differences between Cd and Zn in forming stable $W(CO)_x$ adducts are detailed in Figure 5-1. Additionaly, the **$[Cd\text{-}1']_x$** analog was only isolable as a monodentate ligand to $W(CO)_5$ moiety with no trace of the Cl^- anion that was evinced to cleave and solubilize the coordination polymer.

The nature of this preference is currently unknown, but due to other synthetic works[20] one hypothesis can be made. When a single acetylate arm is attached to the ZnN_2S_2 complex, it deactivates one thiolate, leaving only one $S_{thiolate}$ available to bind to the $W(CO)_5$ complex. This is not entirely without precedence as acetylate arms have been used as protecting groups for thiols in organic and biological synthesis. If it is assumed that the acetylate arm is protecting the non tungsten-complex bound sulfur, then one could hypothesize that the reason the monodentate ZnN_2S_2 complex is unstable is that the free thiolate is responsible for the decomposition of said complex. The cadmium(II) complex displays a similar thiolate reactivity. Whereas the monodentate **$[(Zn\text{-}1'\text{-}Cl)W(CO)_5]^-$** complex's reactivity led to decomposition, the cadmium(II) version is found as a dimer, with the 'free' thiolate bridging to a second molecule's

cadmium ion center. Contrastingly, the bidentate bimetallic complex with cadmium(II) proved to be unisolable, favoring the conversion to the dimeric monodentate tungsten complex.

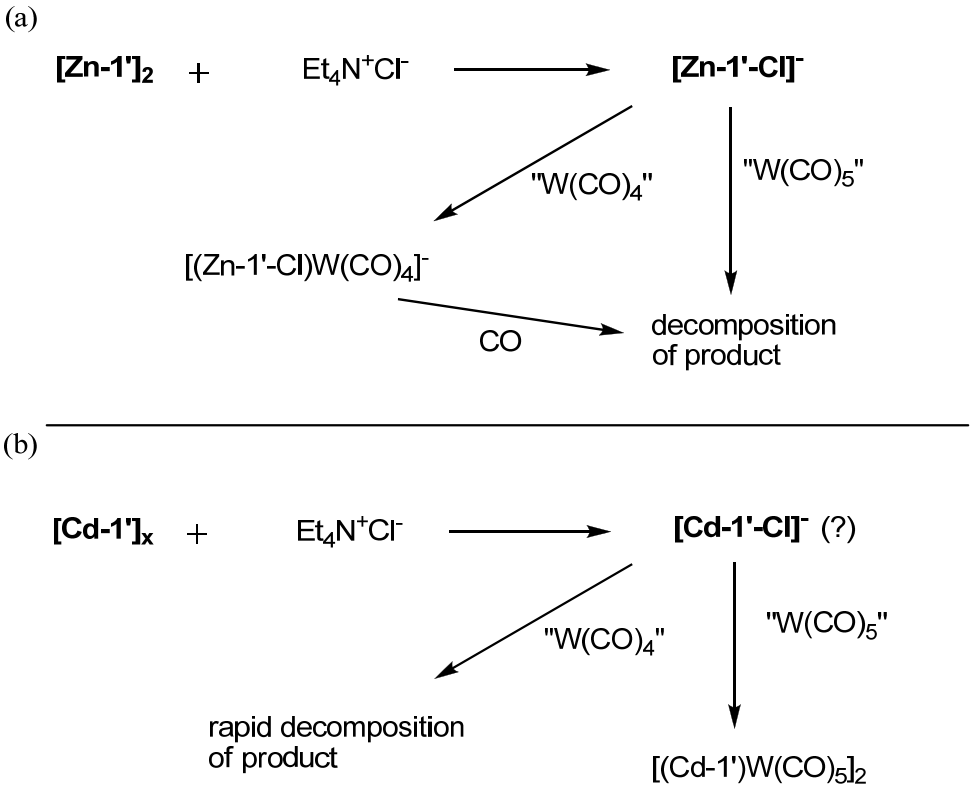

Figure 5-1. A reaction scheme detailing the differences in the synthetic pathways of Zn and Cd complexes to form $W(CO)_x$ adduct complexes.

These findings, when coupled with the geometric discrepancies between **[Zn-1']$_2$** and **[Cd-1']$_x$** reveal the final piece of information that these zinc/cadmium studies have provided. Although the cadmium analogs share some similarities to the zinc complexes they were intended to mirror, their geometric preferences are different enough that any

such use of Cd^{2+} as an analog to Zn^{2+} must be carefully weighed against the possible differences.

The investigation into the metal exchange of **Zn-1'-Ac$_2$** with exogenous metal sources proved enlightening towards the mechanism by which the polydentate ligand system can unwrap from one ion in order to encompass a new one. Additionally, an understanding of a novel new ligand cannibalization process has begun.

We have demonstrated several pathways through which a metal ion can be ligated by the **1'-Ac$_2$** ligand, Figure 5-2. Though it was viable to synthesize the nickel and cobalt complexes via pathway a → b, copper and cadmium both produced too many other products that lowered yield and purity when following that path. The path e was designed so as to ligate the metal ions that proved either impossible or simply messy along the a → b path. Path e, directly synthesizing the hexadentate ligand and then attaching it to a metal ion, not only was able to bind to Cu^{2+} but also to produce the M-1'-Ac_2 complexes of numerous metal ions with both ease and a lack of side products, making it an ideal pathway for future synthesis of six coordinate complexes with this ligand set.

The lack of reactivity towards ion exchange when a $[Zn\text{-}1']_2$ is treated with Ni^{2+}, (pathway d of Figure 5-2) in contrast to the rapid reaction of Ni^{2+} salts with Zn-1'-Ac_x (x = 1 or 2) (pathway c) indicates that the process for ligand unwrapping is based in the interaction of the carboxylate oxygen with the free metal ion.

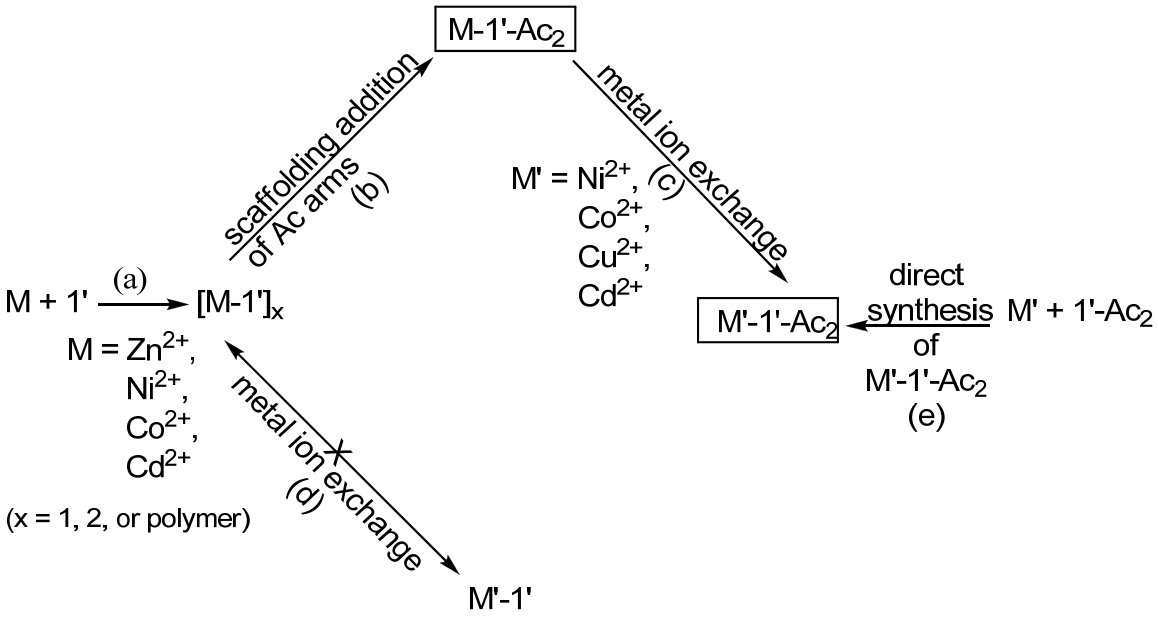

Figure 5-2. The reaction pathways that lead to M'-1'-Ac_2, M'=Ni^{2+}, Co^{2+}, Cu^{2+}, Cd^{2+}.

As for the pathway through which the ligand cannibalism occurs, it is now understood not to be a simple acetylate transfer reaction. If that were the case, **Zn-1'-Ac** would have been able to transfer acetylate arms to the **Ni-1'** complex, but no such reactivity was observed. In order for the acetylate arm to be transferred to a MN_2S_2 complex, it was first necessary to alkylate one of the $S_{thiolate}$ donor atoms, thereby making the metal center more electrophilic towards ancillary carboxylate atoms. This explains why nickel, zinc, cobalt, and cadmium, when bound in the monoacetylated N_2S_2 complex, undergo cannibalism towards other monoacetate complexes to yield the hexacoordinate complexes.

The preliminary results of the screening tests revealed that Co^{2+}, Ni^{2+}, Cu^{2+}, Cd^{2+}, and Hg^{2+} can undergo metal ion exchange with Zn^{2+} in Zn-1'-Ac_2. What is of interest in these findings is the proximity of the metals on the periodic table, Figure 5-3.

The 3rd row metal (II) ions all have very similar ionic radii , .65-.72 Å, making ionic radii seem a possible factor in what metals can exchange with zinc, but then Cd^{2+} 's .97 Å and Hg^{2+} 's 1.1Å radii do not fit within that assumption's parameters. Also, each period has very different preferences towards reactivity and oxidation state possibilities. One commonality is that all of the ions that could exchange with zinc (II) also bind to ethylenediaminetetracetic acid ($EDTA^{4-}$) tighter than does Zn^{2+}. The second observed common point between the listed metal ions was that they all displayed similar electronic effects on the ν(CO) stretching region of the IR spectra.

The direct synthesis of **Cu-1'-Ac$_2$** revealed a further discrepancy between the metal ions. Whereas the Zn^{2+} and Ni^{2+} complexes could be synthesized using the metal as a scaffold for stepwise construction of the ligand by first binding H_2bme-dach and subsequently addition of acetylate arms, Cu^{2+} could only be obtained within the $N_2S_2O_2$ core by exchange or via synthesizing the entire free ligand before adding the copper source. This does provide another example of zinc being used as a scaffold for ligand synthesis so that said ligand may be transferred to a metal that cannot have the ligand built around it.

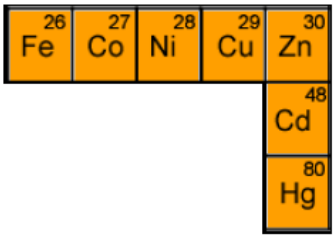

Figure 5-3. M^{2+} ions that were found to undergo direct exchange with **Zn-1'-Ac$_2$**

Altogether, the work presented herein has led to a greater understanding for the use of zinc (II) in biomimetic chemistry. The use of zinc thiolate complexes as donor ligands to tungsten carbonyl complexes was explored and an understanding of the ability of zinc and cadmium thiolate complexes to stably bind to $W(CO)_x$ was garnered. The ability of zinc to act as a scaffold for ligand synthesis and subsequent transfer of the same ligand to exogenous metal ion sources was investigated.

REFERENCES

1. Berg, J. M.; Godwin, H. A. *Annu. Rev. Biophys. Biomol. Struct.* **1997**, *26*, 357-371.

2. Parkin, G. *Chem. Rev.*, **2004**, *104*, 699-767.

3. Wolfe, S.A.; Grant, R.A.; Elrod-Erickson, M.; Pabo, C.O. *Structure* **2001**, *9*, 717–723.

4. Laity, J.H.; Lee, B.M.; Wright, P.E. *Curr. Opin. Struct. Biol.* **2001**, *11*, 39–46.

5. Leon, O.; Roth, M. *Biol. Res.* **2000**, *33*, 21–30.

6. Klug, A.; Schwabe, J.W. *FASEB J.* **1995**, *9*, 597–604.

7. Iuchi S. *Cell. Mol. Life Sci.* **2001**, *58*, 625–635.

8. Krishna, S.; Majumdar, I.; Grishin, N. *Nuc. Acid Res.* **2003**, *31,* 532-550.

9. Maret, W. *Biochemistry* **2004**, *43*, 3301–3309.

10. Matthews, R.G.; Goulding, C.W. *Curr. Opin. Chem. Biol.* **1997**, *1*, 332–339.

11. Hightower, K.E.; Fierke, C.A. *Curr. Opin. Chem. Biol.* **1999**, *3*, 176–181.

12. Smee, J.; Miller, M.; Grapperhaus, C.; Reibenspies, J.H.; and Darensbourg, M.Y. *Inorg. Chem.* **2001**, *40*, 3601-3605.

13. Farmer, P.; Reibenspies, J.H.; Lindahl, P.A.; Darensbourg, M.Y. *J. Am. Chem. Soc.* **1993**, *115*, 4665.

14. Musie, G.; Farmer, P.; Tuntulani, T.; Reibenspies, J.; Darensbourg, M. *Inorg. Chem.* **1996**, *35*, 2176.

15. Grapperhaus, C.; Darensbourg, M.Y. *Acc. Chem. Res.* **1998**, *31*, 451.

16. Emsley, J. *Nature's Building Blocks: An A-Z Guide to the Elements;* Oxford University Press: Oxford, U.K., **2003**; pp 499-505.

17. Berg, J.M.; Shi, Y. *Science* **1996**, *271*, 1081–1085.

18. Maret, W. Antioxid. *Redox Signaling* **2006**, *8*, 1419–1441.

19. Karlin, S.; Zhu, Z.-Y. *Natl. Acad. Sci. U.S.A.* **1997**, *94*, 14231–14236.

20. Almaraz, E.; Foley, W.S.; Denny, J.; Reibenspies, J.; Golden, M.; Darensbourg, M.Y. *Inorg. Chem.* **2009**, *48*, 5288-5295.

21. Rampersad, M.; Jeffery, S.; Golden, M.; Lee, J.; Reibenspies, J.; Darensbourg, D.; Darensbourg, M.Y. *J. Am. Chem. Soc.* **2005***, 127,* 17323-17334.

22. Almaraz, E.; de Paulo, Q.; Liu, Q.; Reibenspies, J.; Darensbourg, M.; Farrell, N. *J. Am. Chem. Soc.* **2008**, *130*, 6272-6280.

23. Meyer, C.; Joiner, C.; Stoddart, F. *Chem. Soc. Rev.* **2007**, *36*, 1705-1723.

24. Gordon, A.J.; Ford, R.A. *The Chemist's Companion*; Wiley and Sons: New York. **1972**; 429-436.

25. Darensbourg, D. J.; Kump, R. L. *Inorg. Chem*. **1978**, *17*, 2680–2682.

26. Sheldrick, G. Acta Crystallogr. **2008**, *A64*, 112–122 and references cited therein.

27. SAINT; Bruker-Nonius Inc.: Madison, WI, 2003.

28. Sheldrick, G. SADABS; University of Göttingen: Göttingen, Germany, 2006.

29. Barbour, L. J. J. *Supramol. Chem.* **2001**, *1*, 189–191.

30. Almaraz, E.; Denny, J. A.; Foley, W.S.; Reibenspies, J. H.; Bhuvanesh, N.; Darensbourg, M. Y. *J. Chem. Soc., Dalton Trans.* **2009,** DOI: 10.1039/b914422f.

31. Pandey, A. S. ; Harris, T. V.; Giles, L. J.; Peters, J. W. Szilagyi, R. K. *J. Am. Chem. Soc.* **2008,** *130*, 4533.

32. Liu, T.; Darensbourg, M.Y. *J. Am. Chem. Soc.* **2007**, *129,* 7008-7009.

33. Bramlett, M.R.; Tan, X.; Lindahl, P.A. *J. Am. Chem. Soc.* **2003**, *125*, 9316-9317.

34. Graperhaus, C.; Tuntulani, T.; Reibenspies, J.; Darensbourg, M. *Inorg. Chem.* **1998**, *37*, 4052-4058.

35. Addison, A. W.; Rao, T. N.; Reedijk, J.; van Rijn, J.; Verschoor, G. C. *J. Chem. Soc., Dalton Trans.* **1984**, *7*, 1349–1356.

36. Chalaca, M. Z.; Figueroa-Villar, J.D.; Ellena, J.A.; Castellano, E.E. *Inorg. Chem. Actica*. **2002**, *328,* 45-52.

37. Darensbour, D.J.; Niezgoda, S.A.; Draper, J.D.; Reibenspies, J.H. *J. Am. Chem. Soc.* **1998**, *120,* 4690-4698.

38. Cotton, F.A.; Kraihanzel, C.S. *J. Am. Chem. Soc.* **1962**, *84*, 4432–4438.

39. Phelps, A.L.; Rampersad, M.V.; Fitch, S. B.; Darensbourg, M.Y.; Darensbourg, D. J. *Inorg. Chem.* **2006**, *45*, 119–126.

40. Rampersad, M.V.; Jeffery, S.P.; Reibenspies, J.H.; Ortiz, C.G.; Darensbourg, D.J.; Darensbourg, M.Y. *Angew. Chem., Int. Ed.* **2005**, *44*, 1217–1220.

41. Anzellotti, A.; Liu, Q.; Bloemink, M.; Scarsdale, J.; Farrell, N. *Chem. Biol.* **2006**, *13*, 1-10.

42. Liu, Q.; Golden, M.; Darensbourg, M.; Farrell, N. *Chem. Commun.* **2006**, *34*, 4360-4362.

43. Emsley, J. *The Elements* 3rd ed., Clarendon Press: Oxford, UK, **1998**.

44. Doukov, T.I.; Iverson, T.M.; Seravalli, J.; Ragsdale, S.W.; Drennan, C.L. *Science* **2002**, *298*, 567.

45. Darnault, C.; Volbeda, A.; Kim, E.J.; Legrand, P.; Vernede, X.; Lindahl, P.A.; Fontecilla-Camps, J.C. *Nat. Struct. Biol.* **2003,** *10***,** 271-279.

46. Shin, W; Anderson, M.E.; Lindahl, P.A. *J. Am. Chem. Soc.* **1993**, *115*, 5522-5526.

47. Goodman, D.C.; Tuntulani, T.; Farmer, P.J.; Reibenspies, J.H.; and Darensbourg, M.Y. *Angew. Chem., Int. Ed. Engl.*, **1993**, *32*, 116–119.

47b. Goodman, D.C.; Farmer, P. J.; Reibenspies, J.H.; and Darensbourg, M.Y. *Inorg. Chem.*, **1996**, *35*, 4989–4994.

48. Miller, M.L.; Ibrahim, S.A.; Golden, M.L.; Darensbourg, M.Y. *Inorg. Chem.* **2003**, *42*, 2999-3007.

49. Bydalek, T.J.; Margerum, D.W. *Inorg. Chem.* **1963**, *2*, 678–683.

50. Margerum, D.W.; Janes, D.L.; Rosen, H.M. *J. Am. Chem. Soc.* **1965**, *87*, 4463–4472.

51. Voet, D.; Voet, J.G.; Pratt, C.W. *Fundementals of Biochemistry;* Wiley & Sons: New York, **2002**; pp282-284.

52. Darnault, C.; Volbeda, A.; Kim, E.J.; Legrand, P.; Vernede, X.; Lindahl, P.A.; Fontecilla-Camps, J.C. *Nat Struct. Biol.* **2003,** *10*, 271-279.

53. Nagashima, S.; Nakasako, M.; Dohmae, N.; Tsujimura, M.; Takio, K.; Odaka, M.; Yohda, M.; Kamiya, N.; Endo, I. *Nat. Struct. Biol.* **1998**, *5*, 347-351.

54. Barondeau, D.P.; Kassmann, C.J.; Bruns, C.K.; Tainer, J.A.; Getzoff, E.D. *Biochemistry* **2004**, *43,* 8038-8047.

55. Choudhury, S.B.; Davidson, G.; Yim, Y.; Bose, K.; Sharma, M.L.; Kang, S.O.; Cabelli, D.E.; Maroney, M.J. *Biochemistry,* **1999**, *38*, 3744-3752.

APPENDIX A

CRYSTALLOGRAPHIC DATA FOR STRUCTURES

$[Et_4N][(Zn\text{-}1'\text{-}Cl)W(CO)_4]$

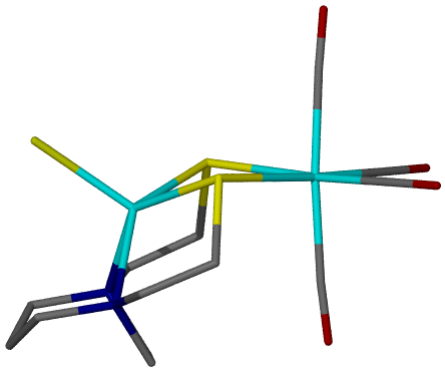

$[Cd\text{-}1']_x$

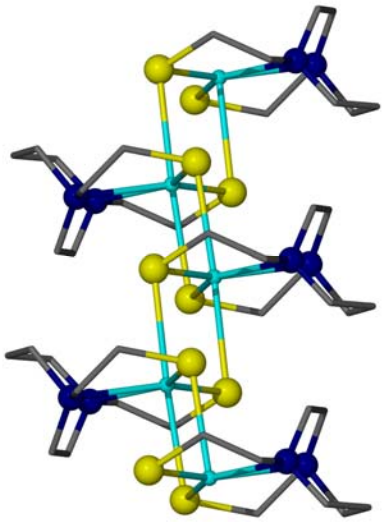

$[(Cd\text{-}1')W(CO)_5]_2$

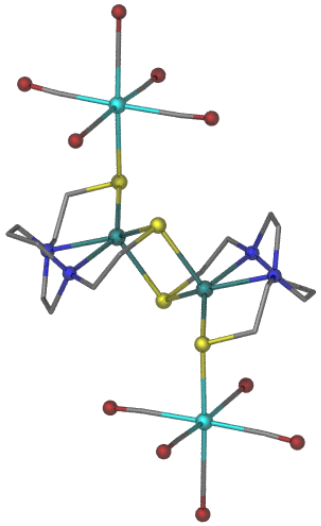

Table A-1. Crystal data and structure refinement for **[Et_4N][(Zn-1'-Cl)$W(CO)_4$].**

Empirical formula	C21.50 H41 Cl2 N3 O5 S2 W Zn	
Formula weight	805.81	
Temperature	110(2) K	
Wavelength	0.71073 Å	
Crystal system	Monoclinic	
Space group	C2/c	
Unit cell dimensions	a = 23.781(3) Å	a= 90°.
	b = 8.5401(12) Å	b= 107.227(2)°.
	c = 30.599(4) Å	g = 90°.
Volume	5935.5(15) $Å^3$	
Z	8	
Density (calculated)	1.803 Mg/m^3	
Absorption coefficient	5.037 mm^{-1}	
F(000)	3208	
Crystal size	0.20 x 0.10 x 0.10 mm^3	
Theta range for data collection	2.55 to 25.00°.	
Index ranges	-28<=h<=28, -10<=k<=10, -36<=l<=36	
Reflections collected	26462	
Independent reflections	5106 [R(int) = 0.1190]	
Completeness to theta = 25.00°	97.8 %	
Absorption correction	Semi-empirical from equivalents	
Max. and min. transmission	0.6328 and 0.4324	
Refinement method	Full-matrix least-squares on F^2	
Data / restraints / parameters	5106 / 0 / 324	
Goodness-of-fit on F^2	1.019	
Final R indices [I>2sigma(I)]	R1 = 0.0301, wR2 = 0.0612	
R indices (all data)	R1 = 0.0374, wR2 = 0.0633	
Largest diff. peak and hole	1.980 and -1.486 e.$Å^{-3}$	

Table A-2. Bond lengths [Å] and angles [°] for **[Et_4N][(Zn-1'-Cl)$W(CO)_4$].**

W(1)-C(12)	1.950(5)
W(1)-C(11)	1.962(5)
W(1)-C(13)	2.012(5)
W(1)-C(10)	2.041(5)
W(1)-S(2)	2.5912(11)
W(1)-S(1)	2.5915(11)
Zn(1)-N(2)	2.182(3)
Zn(1)-N(1)	2.232(4)
Zn(1)-Cl(1)	2.2902(12)
Zn(1)-S(1)	2.3845(11)
Zn(1)-S(2)	2.4055(12)
ClM-C(1M)	1.582(13)
ClM-C(1M)#1	1.695(11)
C(1M)-C(1M)#1	1.42(2)
C(1M)-ClM#1	1.695(11)
C(1M)-H(1MA)	0.9600
C(1M)-H(1MB)	0.9599
O(1W)-H(1W1)	0.8500
O(1W)-H(2W1)	0.8500
S(2)-C(1)	1.834(4)
S(1)-C(9)	1.830(5)
O(3)-C(12)	1.166(5)
O(2)-C(11)	1.160(5)
O(4)-C(13)	1.152(6)
O(1)-C(10)	1.154(5)
N(1)-C(4)	1.473(5)
N(1)-C(8)	1.480(5)
N(1)-C(7)	1.492(5)
N(2)-C(3)	1.465(6)
N(2)-C(2)	1.473(6)
N(2)-C(5)	1.491(5)
N(3)-C(18)	1.515(6)

(Table A-2 continued)

N(3)-C(14)	1.517(6)
N(3)-C(16)	1.521(6)
N(3)-C(20)	1.523(5)
C(1)-C(2)	1.517(6)
C(1)-H(1A)	0.9900
C(1)-H(1B)	0.9900
C(2)-H(2A)	0.9900
C(2)-H(2B)	0.9900
C(3)-C(4)	1.551(6)
C(3)-H(3A)	0.9900
C(3)-H(3B)	0.9900
C(4)-H(4A)	0.9900
C(4)-H(4B)	0.9900
C(5)-C(6)	1.545(7)
C(5)-H(5A)	0.9900
C(5)-H(5B)	0.9900
C(6)-C(7)	1.514(6)
C(6)-H(6A)	0.9900
C(6)-H(6B)	0.9900
C(7)-H(7A)	0.9900
C(7)-H(7B)	0.9900
C(8)-C(9)	1.521(6)
C(8)-H(8A)	0.9900
C(8)-H(8B)	0.9900
C(9)-H(9A)	0.9900
C(9)-H(9B)	0.9900
C(14)-C(15)	1.506(7)
C(14)-H(14A)	0.9900
C(14)-H(14B)	0.9900
C(15)-H(15A)	0.9800
C(15)-H(15B)	0.9800
C(15)-H(15C)	0.9800

(Table A-2 continued)

C(16)-C(17)	1.520(6)
C(16)-H(16A)	0.9900
C(16)-H(16B)	0.9900
C(17)-H(17A)	0.9800
C(17)-H(17B)	0.9800
C(17)-H(17C)	0.9800
C(18)-C(19)	1.496(6)
C(18)-H(18A)	0.9900
C(18)-H(18B)	0.9900
C(19)-H(19A)	0.9800
C(19)-H(19B)	0.9800
C(19)-H(19C)	0.9800
C(20)-C(21)	1.519(6)
C(20)-H(20A)	0.9900
C(20)-H(20B)	0.9900
C(21)-H(21A)	0.9800
C(21)-H(21B)	0.9800
C(21)-H(21C)	0.9800

C(12)-W(1)-C(11)	89.56(18)
C(12)-W(1)-C(13)	88.65(18)
C(11)-W(1)-C(13)	86.74(18)
C(12)-W(1)-C(10)	90.35(18)
C(11)-W(1)-C(10)	86.80(18)
C(13)-W(1)-C(10)	173.48(16)
C(12)-W(1)-S(2)	92.72(13)
C(11)-W(1)-S(2)	176.61(13)
C(13)-W(1)-S(2)	95.82(12)
C(10)-W(1)-S(2)	90.67(12)
C(12)-W(1)-S(1)	174.00(14)
C(11)-W(1)-S(1)	95.23(13)
C(13)-W(1)-S(1)	95.21(12)

(Table A-2 continued)

C(10)-W(1)-S(1)	86.32(12)
S(2)-W(1)-S(1)	82.34(3)
N(2)-Zn(1)-N(1)	73.21(13)
N(2)-Zn(1)-Cl(1)	106.44(10)
N(1)-Zn(1)-Cl(1)	107.24(9)
N(2)-Zn(1)-S(1)	140.84(11)
N(1)-Zn(1)-S(1)	85.07(9)
Cl(1)-Zn(1)-S(1)	111.02(4)
N(2)-Zn(1)-S(2)	86.83(10)
N(1)-Zn(1)-S(2)	141.44(9)
Cl(1)-Zn(1)-S(2)	109.97(5)
S(1)-Zn(1)-S(2)	90.84(4)
C(1M)-ClM-C(1M)#1	51.0(7)
C(1M)#1-C(1M)-ClM	68.6(10)
C(1M)#1-C(1M)-ClM#1	60.4(8)
ClM-C(1M)-ClM#1	129.0(7)
C(1M)#1-C(1M)-H(1MA)	122.3
ClM-C(1M)-H(1MA)	101.9
ClM#1-C(1M)-H(1MA)	104.7
C(1M)#1-C(1M)-H(1MB)	131.4
ClM-C(1M)-H(1MB)	105.5
ClM#1-C(1M)-H(1MB)	107.6
H(1MA)-C(1M)-H(1MB)	106.3
H(1W1)-O(1W)-H(2W1)	114.9
C(1)-S(2)-Zn(1)	95.49(14)
C(1)-S(2)-W(1)	111.45(16)
Zn(1)-S(2)-W(1)	89.24(4)
C(9)-S(1)-Zn(1)	97.76(14)
C(9)-S(1)-W(1)	111.93(16)
Zn(1)-S(1)-W(1)	89.69(4)
C(4)-N(1)-C(8)	112.0(3)
C(4)-N(1)-C(7)	110.6(3)

(Table A-2 continued)

C(8)-N(1)-C(7)	109.3(3)
C(4)-N(1)-Zn(1)	106.9(2)
C(8)-N(1)-Zn(1)	110.0(3)
C(7)-N(1)-Zn(1)	107.9(3)
C(3)-N(2)-C(2)	112.0(3)
C(3)-N(2)-C(5)	110.5(4)
C(2)-N(2)-C(5)	110.0(3)
C(3)-N(2)-Zn(1)	108.5(2)
C(2)-N(2)-Zn(1)	108.1(3)
C(5)-N(2)-Zn(1)	107.7(3)
C(18)-N(3)-C(14)	107.2(4)
C(18)-N(3)-C(16)	111.2(3)
C(14)-N(3)-C(16)	110.9(3)
C(18)-N(3)-C(20)	111.0(3)
C(14)-N(3)-C(20)	110.5(3)
C(16)-N(3)-C(20)	106.0(3)
C(2)-C(1)-S(2)	111.0(3)
C(2)-C(1)-H(1A)	109.4
S(2)-C(1)-H(1A)	109.4
C(2)-C(1)-H(1B)	109.4
S(2)-C(1)-H(1B)	109.4
H(1A)-C(1)-H(1B)	108.0
N(2)-C(2)-C(1)	113.4(3)
N(2)-C(2)-H(2A)	108.9
C(1)-C(2)-H(2A)	108.9
N(2)-C(2)-H(2B)	108.9
C(1)-C(2)-H(2B)	108.9
H(2A)-C(2)-H(2B)	107.7
N(2)-C(3)-C(4)	111.7(3)
N(2)-C(3)-H(3A)	109.3
C(4)-C(3)-H(3A)	109.3
N(2)-C(3)-H(3B)	109.3

(Table A-2 continued)

C(4)-C(3)-H(3B)	109.3
H(3A)-C(3)-H(3B)	107.9
N(1)-C(4)-C(3)	111.5(4)
N(1)-C(4)-H(4A)	109.3
C(3)-C(4)-H(4A)	109.3
N(1)-C(4)-H(4B)	109.3
C(3)-C(4)-H(4B)	109.3
H(4A)-C(4)-H(4B)	108.0
N(2)-C(5)-C(6)	112.7(4)
N(2)-C(5)-H(5A)	109.1
C(6)-C(5)-H(5A)	109.1
N(2)-C(5)-H(5B)	109.1
C(6)-C(5)-H(5B)	109.0
H(5A)-C(5)-H(5B)	107.8
C(7)-C(6)-C(5)	116.1(4)
C(7)-C(6)-H(6A)	108.3
C(5)-C(6)-H(6A)	108.3
C(7)-C(6)-H(6B)	108.3
C(5)-C(6)-H(6B)	108.3
H(6A)-C(6)-H(6B)	107.4
N(1)-C(7)-C(6)	112.8(3)
N(1)-C(7)-H(7A)	109.0
C(6)-C(7)-H(7A)	109.0
N(1)-C(7)-H(7B)	109.0
C(6)-C(7)-H(7B)	109.0
H(7A)-C(7)-H(7B)	107.8
N(1)-C(8)-C(9)	112.0(3)
N(1)-C(8)-H(8A)	109.2
C(9)-C(8)-H(8A)	109.2
N(1)-C(8)-H(8B)	109.2
C(9)-C(8)-H(8B)	109.2
H(8A)-C(8)-H(8B)	107.9

(Table A-2 continued)

C(8)-C(9)-S(1)	111.8(3)
C(8)-C(9)-H(9A)	109.3
S(1)-C(9)-H(9A)	109.3
C(8)-C(9)-H(9B)	109.3
S(1)-C(9)-H(9B)	109.3
H(9A)-C(9)-H(9B)	107.9
O(1)-C(10)-W(1)	175.5(4)
O(2)-C(11)-W(1)	179.5(5)
O(3)-C(12)-W(1)	179.4(5)
O(4)-C(13)-W(1)	175.7(4)
C(15)-C(14)-N(3)	115.2(4)
C(15)-C(14)-H(14A)	108.5
N(3)-C(14)-H(14A)	108.5
C(15)-C(14)-H(14B)	108.5
N(3)-C(14)-H(14B)	108.5
H(14A)-C(14)-H(14B)	107.5
C(14)-C(15)-H(15A)	109.5
C(14)-C(15)-H(15B)	109.5
H(15A)-C(15)-H(15B)	109.5
C(14)-C(15)-H(15C)	109.5
H(15A)-C(15)-H(15C)	109.5
H(15B)-C(15)-H(15C)	109.5
C(17)-C(16)-N(3)	114.2(4)
C(17)-C(16)-H(16A)	108.7
N(3)-C(16)-H(16A)	108.7
C(17)-C(16)-H(16B)	108.7
N(3)-C(16)-H(16B)	108.7
H(16A)-C(16)-H(16B)	107.6
C(16)-C(17)-H(17A)	109.5
C(16)-C(17)-H(17B)	109.5
H(17A)-C(17)-H(17B)	109.5
C(16)-C(17)-H(17C)	109.5

(Table A-2 continued)

H(17A)-C(17)-H(17C)	109.5
H(17B)-C(17)-H(17C)	109.5
C(19)-C(18)-N(3)	116.3(4)
C(19)-C(18)-H(18A)	108.2
N(3)-C(18)-H(18A)	108.2
C(19)-C(18)-H(18B)	108.2
N(3)-C(18)-H(18B)	108.2
H(18A)-C(18)-H(18B)	107.4
C(18)-C(19)-H(19A)	109.5
C(18)-C(19)-H(19B)	109.5
H(19A)-C(19)-H(19B)	109.5
C(18)-C(19)-H(19C)	109.5
H(19A)-C(19)-H(19C)	109.5
H(19B)-C(19)-H(19C)	109.5
C(21)-C(20)-N(3)	114.7(4)
C(21)-C(20)-H(20A)	108.6
N(3)-C(20)-H(20A)	108.6
C(21)-C(20)-H(20B)	108.6
N(3)-C(20)-H(20B)	108.6
H(20A)-C(20)-H(20B)	107.6
C(20)-C(21)-H(21A)	109.5
C(20)-C(21)-H(21B)	109.5
H(21A)-C(21)-H(21B)	109.5
C(20)-C(21)-H(21C)	109.5
H(21A)-C(21)-H(21C)	109.5
H(21B)-C(21)-H(21C)	109.5

Symmetry transformations used to generate equivalent atoms:
#1 -x+1/2,-y-1/2,-z

Table A-3. Crystal data and structure refinement for **$[Cd\text{-}1']_x$.**

Empirical formula	C9 H18 Cd N2 S2	
Formula weight	330.77	
Temperature	110(2) K	
Wavelength	1.54184 Å	
Crystal system	Monoclinic	
Space group	C2/c	
Unit cell dimensions	a = 14.690(5) Å	a= 90°.
	b = 11.059(3) Å	b= 110.033(15)°.
	c = 7.516(2) Å	g = 90°.
Volume	1147.1(6) $Å^3$	
Z	4	
Density (calculated)	1.915 Mg/m^3	
Absorption coefficient	18.344 mm^{-1}	
F(000)	664	
Crystal size	0.20 x 0.01 x 0.01 mm^3	
Theta range for data collection	7.20 to 59.83°.	
Index ranges	-16<=h<=15, -12<=k<=12, -7<=l<=8	
Reflections collected	3023	
Independent reflections	656 [R(int) = 0.0498]	
Completeness to theta = 59.83°	76.9 %	
Absorption correction	Semi-empirical from equivalents	
Max. and min. transmission	0.8378 and 0.1205	
Refinement method	Full-matrix least-squares on F^2	
Data / restraints / parameters	656 / 16 / 87	
Goodness-of-fit on F^2	1.012	
Final R indices [I>2sigma(I)]	R1 = 0.0253, wR2 = 0.0491	
R indices (all data)	R1 = 0.0346, wR2 = 0.0505	
Largest diff. peak and hole	0.529 and -0.420 $e.Å^{-3}$	

Table A-4. Bond lengths [Å] and angles [°] for **[Cd-1']$_x$.**

Cd(1)-N(1)#1	2.496(4)
Cd(1)-N(1)	2.496(4)
Cd(1)-S(1)	2.5620(12)
Cd(1)-S(1)#1	2.5620(12)
Cd(1)-S(1)#2	2.8417(14)
Cd(1)-S(1)#3	2.8417(14)
S(1)-C(1)	1.815(6)
S(1)-Cd(1)#3	2.8417(14)
N(1)-C(7)#1	1.420(13)
N(1)-C(4)#1	1.425(18)
N(1)-C(2)	1.474(8)
N(1)-C(5)	1.551(11)
N(1)-C(3)	1.557(11)
C(1)-C(2)	1.472(10)
C(1)-H(1A)	0.9900
C(1)-H(1B)	0.9900
C(2)-H(2A)	0.9900
C(2)-H(2B)	0.9900
C(3)-C(4)	1.522(10)
C(3)-H(3A)	0.9900
C(3)-H(3B)	0.9900
C(4)-N(1)#1	1.425(18)
C(4)-H(4A)	0.9900
C(4)-H(4B)	0.9900
C(5)-C(6)	1.520(10)
C(5)-H(5A)	0.9900
C(5)-H(5B)	0.9900
C(6)-C(7)	1.517(10)
C(6)-H(6A)	0.9900
C(6)-H(6B)	0.9900
C(7)-N(1)#1	1.420(13)
C(7)-H(7A)	0.9900

(Table A-4 continued)

C(7)-H(7B)	0.9900
N(1)#1-Cd(1)-N(1)	64.9(2)
N(1)#1-Cd(1)-S(1)	145.87(11)
N(1)-Cd(1)-S(1)	81.48(11)
N(1)#1-Cd(1)-S(1)#1	81.48(11)
N(1)-Cd(1)-S(1)#1	145.87(11)
S(1)-Cd(1)-S(1)#1	132.50(5)
N(1)#1-Cd(1)-S(1)#2	86.21(10)
N(1)-Cd(1)-S(1)#2	96.02(10)
S(1)-Cd(1)-S(1)#2	91.64(4)
S(1)#1-Cd(1)-S(1)#2	87.30(4)
N(1)#1-Cd(1)-S(1)#3	96.02(10)
N(1)-Cd(1)-S(1)#3	86.21(10)
S(1)-Cd(1)-S(1)#3	87.30(4)
S(1)#1-Cd(1)-S(1)#3	91.64(4)
S(1)#2-Cd(1)-S(1)#3	177.37(5)
C(1)-S(1)-Cd(1)	93.97(19)
C(1)-S(1)-Cd(1)#3	105.2(3)
Cd(1)-S(1)-Cd(1)#3	92.70(4)
C(7)#1-N(1)-C(4)#1	117.2(11)
C(7)#1-N(1)-C(2)	94.2(7)
C(4)#1-N(1)-C(2)	114.9(6)
C(7)#1-N(1)-C(5)	115.4(9)
C(4)#1-N(1)-C(5)	10.5(9)
C(2)-N(1)-C(5)	105.4(6)
C(7)#1-N(1)-C(3)	32.4(5)
C(4)#1-N(1)-C(3)	104.0(9)
C(2)-N(1)-C(3)	125.5(7)
C(5)-N(1)-C(3)	108.2(8)
C(7)#1-N(1)-Cd(1)	122.0(5)
C(4)#1-N(1)-Cd(1)	101.9(9)

(Table A-4 continued)

C(2)-N(1)-Cd(1)	106.7(3)
C(5)-N(1)-Cd(1)	110.0(8)
C(3)-N(1)-Cd(1)	100.5(5)
C(2)-C(1)-S(1)	115.1(5)
C(2)-C(1)-H(1A)	108.5
S(1)-C(1)-H(1A)	108.5
C(2)-C(1)-H(1B)	108.5
S(1)-C(1)-H(1B)	108.5
H(1A)-C(1)-H(1B)	107.5
C(1)-C(2)-N(1)	116.6(6)
C(1)-C(2)-H(2A)	108.1
N(1)-C(2)-H(2A)	108.1
C(1)-C(2)-H(2B)	108.1
N(1)-C(2)-H(2B)	108.1
H(2A)-C(2)-H(2B)	107.3
C(4)-C(3)-N(1)	114.0(11)
C(4)-C(3)-H(3A)	108.8
N(1)-C(3)-H(3A)	108.8
C(4)-C(3)-H(3B)	108.8
N(1)-C(3)-H(3B)	108.8
H(3A)-C(3)-H(3B)	107.6
N(1)#1-C(4)-C(3)	111.2(12)
N(1)#1-C(4)-H(4A)	109.4
C(3)-C(4)-H(4A)	109.4
N(1)#1-C(4)-H(4B)	109.4
C(3)-C(4)-H(4B)	109.4
H(4A)-C(4)-H(4B)	108.0
C(6)-C(5)-N(1)	114.2(9)
C(6)-C(5)-H(5A)	108.7
N(1)-C(5)-H(5A)	108.7
C(6)-C(5)-H(5B)	108.7
N(1)-C(5)-H(5B)	108.7

(Table A-4 continued)

H(5A)-C(5)-H(5B)	107.6
C(7)-C(6)-C(5)	117.0(11)
C(7)-C(6)-H(6A)	108.0
C(5)-C(6)-H(6A)	108.0
C(7)-C(6)-H(6B)	108.0
C(5)-C(6)-H(6B)	108.0
H(6A)-C(6)-H(6B)	107.3
N(1)#1-C(7)-C(6)	106.8(10)
N(1)#1-C(7)-H(7A)	110.4
C(6)-C(7)-H(7A)	110.4
N(1)#1-C(7)-H(7B)	110.4
C(6)-C(7)-H(7B)	110.4
H(7A)-C(7)-H(7B)	108.6

Symmetry transformations used to generate equivalent atoms:
#1 -x,y,-z+1/2 #2 x,-y,z-1/2 #3 -x,-y,-z+1

Table A-5. Crystal data and structure refinement for **[(Cd-1')W(CO)$_5$]$_2$.**

Empirical formula	C14 H16 Cd N2 O5 S2 W	
Formula weight	652.66	
Temperature	110(2) K	
Wavelength	1.54178 Å	
Crystal system	Monoclinic	
Space group	P2(1)/c	
Unit cell dimensions	a = 14.574(3) Å	a = 90°.
	b = 11.540(3) Å	b = 115.686(11)°.
	c = 12.711(3) Å	g = 90°.
Volume	1926.5(8) Å^3	
Z	4	
Density (calculated)	2.250 Mg/m^3	
Absorption coefficient	21.983 mm^{-1}	
F(000)	1232	
Crystal size	0.03 x 0.02 x 0.01 mm^3	
Theta range for data collection	3.36 to 60.84°.	
Index ranges	-15<=h<=16, -12<=k<=13, -14<=l<=14	
Reflections collected	14013	
Independent reflections	2868 [R(int) = 0.1997]	
Completeness to theta = 60.84°	97.9 %	
Absorption correction	Semi-empirical from equivalents	
Max. and min. transmission	0.8101 and 0.5584	
Refinement method	Full-matrix least-squares on F^2	
Data / restraints / parameters	2868 / 175 / 226	
Goodness-of-fit on F^2	1.070	
Final R indices [I>2sigma(I)]	R1 = 0.0913, wR2 = 0.2265	
R indices (all data)	R1 = 0.1401, wR2 = 0.2592	
Largest diff. peak and hole	1.939 and -2.371 e.Å^{-3}	

Table A-6. Bond lengths [Å] and angles [°] for **[(Cd-1')W(CO)$_5$]$_2$.**

Cd(1)-N(2)	2.40(2)
Cd(1)-N(1)	2.40(2)
Cd(1)-S(1)	2.527(6)
Cd(1)-S(2)	2.574(6)
Cd(1)-S(2)#1	2.593(6)
S(1)-C(1)	1.86(3)
S(1)-W(1)	2.583(7)
S(2)-C(9)	1.88(3)
S(2)-Cd(1)#1	2.593(6)
N(1)-C(5)	1.30(4)
N(1)-C(3)	1.52(4)
N(1)-C(2)	1.54(3)
N(2)-C(7)	1.46(4)
N(2)-C(8)	1.48(4)
N(2)-C(4)	1.58(4)
C(1)-C(2)	1.50(4)
C(1)-H(1A)	0.9900
C(1)-H(1B)	0.9900
C(2)-H(2A)	0.9900
C(2)-H(2B)	0.9900
C(3)-C(4)	1.65(4)
C(3)-H(3A)	0.9900
C(3)-H(3B)	0.9900
C(4)-H(4A)	0.9900
C(4)-H(4B)	0.9900
C(5)-C(6)	1.37(4)
C(5)-H(5)	0.9500
C(6)-C(7)	1.51(4)
C(6)-H(6)	0.9500
C(7)-H(7A)	0.9900
C(7)-H(7B)	0.9900
C(8)-C(9)	1.49(4)

(Table A-6 continued)

C(8)-H(8A)	0.9900
C(8)-H(8B)	0.9900
C(9)-H(9A)	0.9900
C(9)-H(9B)	0.9900
W(1)-C(14)	1.91(3)
W(1)-C(10)	2.02(3)
W(1)-C(11)	2.05(3)
W(1)-C(13)	2.06(3)
W(1)-C(12)	2.11(3)
C(10)-O(10)	1.13(3)
C(11)-O(11)	1.14(3)
C(12)-O(12)	1.09(3)
C(13)-O(13)	1.10(3)
C(14)-O(14)	1.18(3)

N(2)-Cd(1)-N(1)	65.5(8)
N(2)-Cd(1)-S(1)	142.7(7)
N(1)-Cd(1)-S(1)	82.4(6)
N(2)-Cd(1)-S(2)	81.3(6)
N(1)-Cd(1)-S(2)	143.6(6)
S(1)-Cd(1)-S(2)	121.0(2)
N(2)-Cd(1)-S(2)#1	99.5(7)
N(1)-Cd(1)-S(2)#1	105.4(7)
S(1)-Cd(1)-S(2)#1	107.3(2)
S(2)-Cd(1)-S(2)#1	94.2(2)
C(1)-S(1)-Cd(1)	97.4(9)
C(1)-S(1)-W(1)	109.2(10)
Cd(1)-S(1)-W(1)	112.6(2)
C(9)-S(2)-Cd(1)	97.6(9)
C(9)-S(2)-Cd(1)#1	99.5(11)
Cd(1)-S(2)-Cd(1)#1	85.8(2)
C(5)-N(1)-C(3)	121(3)

(Table A-6 continued)

C(5)-N(1)-C(2)	109(2)
C(3)-N(1)-C(2)	102(2)
C(5)-N(1)-Cd(1)	115(2)
C(3)-N(1)-Cd(1)	105.2(17)
C(2)-N(1)-Cd(1)	102.1(16)
C(7)-N(2)-C(8)	104(2)
C(7)-N(2)-C(4)	115(2)
C(8)-N(2)-C(4)	112(3)
C(7)-N(2)-Cd(1)	110.9(19)
C(8)-N(2)-Cd(1)	108.9(17)
C(4)-N(2)-Cd(1)	105.6(16)
C(2)-C(1)-S(1)	112.8(19)
C(2)-C(1)-H(1A)	109.0
S(1)-C(1)-H(1A)	109.0
C(2)-C(1)-H(1B)	109.0
S(1)-C(1)-H(1B)	109.0
H(1A)-C(1)-H(1B)	107.8
C(1)-C(2)-N(1)	112(2)
C(1)-C(2)-H(2A)	109.3
N(1)-C(2)-H(2A)	109.3
C(1)-C(2)-H(2B)	109.3
N(1)-C(2)-H(2B)	109.3
H(2A)-C(2)-H(2B)	108.0
N(1)-C(3)-C(4)	103(2)
N(1)-C(3)-H(3A)	111.2
C(4)-C(3)-H(3A)	111.2
N(1)-C(3)-H(3B)	111.2
C(4)-C(3)-H(3B)	111.2
H(3A)-C(3)-H(3B)	109.1
N(2)-C(4)-C(3)	112(2)
N(2)-C(4)-H(4A)	109.3
C(3)-C(4)-H(4A)	109.3

(Table A-6 continued)

N(2)-C(4)-H(4B)	109.3
C(3)-C(4)-H(4B)	109.3
H(4A)-C(4)-H(4B)	108.0
N(1)-C(5)-C(6)	113(3)
N(1)-C(5)-H(5)	123.4
C(6)-C(5)-H(5)	123.4
C(5)-C(6)-C(7)	130(3)
C(5)-C(6)-H(6)	114.9
C(7)-C(6)-H(6)	114.9
N(2)-C(7)-C(6)	106(3)
N(2)-C(7)-H(7A)	110.6
C(6)-C(7)-H(7A)	110.6
N(2)-C(7)-H(7B)	110.6
C(6)-C(7)-H(7B)	110.6
H(7A)-C(7)-H(7B)	108.7
N(2)-C(8)-C(9)	116(3)
N(2)-C(8)-H(8A)	108.4
C(9)-C(8)-H(8A)	108.4
N(2)-C(8)-H(8B)	108.4
C(9)-C(8)-H(8B)	108.4
H(8A)-C(8)-H(8B)	107.4
C(8)-C(9)-S(2)	115(2)
C(8)-C(9)-H(9A)	108.6
S(2)-C(9)-H(9A)	108.6
C(8)-C(9)-H(9B)	108.6
S(2)-C(9)-H(9B)	108.6
H(9A)-C(9)-H(9B)	107.5
C(14)-W(1)-C(10)	87.2(13)
C(14)-W(1)-C(11)	91.5(11)
C(10)-W(1)-C(11)	89.1(14)
C(14)-W(1)-C(13)	92.0(12)
C(10)-W(1)-C(13)	91.9(15)

(Table A-6 continued)

C(11)-W(1)-C(13)	176.3(11)
C(14)-W(1)-C(12)	91.4(12)
C(10)-W(1)-C(12)	178.5(13)
C(11)-W(1)-C(12)	91.6(13)
C(13)-W(1)-C(12)	87.5(15)
C(14)-W(1)-S(1)	178.0(9)
C(10)-W(1)-S(1)	94.4(10)
C(11)-W(1)-S(1)	89.6(8)
C(13)-W(1)-S(1)	86.8(9)
C(12)-W(1)-S(1)	87.0(9)
O(10)-C(10)-W(1)	175(3)
O(11)-C(11)-W(1)	174(3)
O(12)-C(12)-W(1)	174(3)
O(13)-C(13)-W(1)	175(3)
O(14)-C(14)-W(1)	178(2)

Symmetry transformations used to generate equivalent atoms:
#1 -x+1,-y+1,-z

VITA

Name:	William Scott Foley
Address:	Department of Chemistry, Texas A&M University PO Box 30012, College Station, TX 77842-3012
Email Address:	likard323@gmail.com
Education:	B.S., Chemistry, Texas A&M University, 2007 M.S., Chemistry, Texas A&M University, 2009